



universität  
wien

# MASTERARBEIT

Titel der Masterarbeit

Diffraction of polarizable and polar molecules at  
ultrathin material gratings

Verfasser

Christian Gerald Knobloch, B.Sc.

Angestrebter akademischer Grad

Master of Science (M.Sc.)

Wien, August 2014

Studienkennzahl lt. Studienblatt: A 066876

Studienrichtung lt. Studienblatt: Masterstudium Physik

Betreuer: Univ.-Prof. Dr. Markus Arndt







# Zusammenfassung

Nanotechnologie wird in der heutigen Zeit in allen Bereichen des Lebens immer wichtiger. Deshalb ist es von großem Nutzen die fundamentalen Kräfte zu verstehen, die in dieser Größenordnung eine Rolle spielen. Die vorliegende Arbeit nutzt die quantenmechanischen Eigenschaften von Materie um Kräfte zwischen Molekülen und Nanostrukturen zu untersuchen. Dazu wird in einem Materiewellen-Interferometer durch ein Interferenzbild erzeugt und mit Hilfe von Fluoreszenzdetektion sichtbar gemacht. Die Wechselwirkungen zwischen dem Strahl aus polarisierbaren und polaren Molekülen und dem beugenden Gitter spiegeln sich dabei im Interferenzmuster wieder. Weiters wurde der Aufbau benutzt um den Streuquerschnitt von Molekülen zu bestimmen sowie den Einfluss von Ladungsträgern am Gitter auf das Interferenzbild zu studieren.

## Abstract

Nanotechnology is becoming more important in daily life. Hence, it is important to acquire fundamental knowledge about forces acting on the nano scale. The presented work combines the quantum mechanical tool of matter wave interferometry with the investigation of forces acting between molecules and nano scale devices. With the setup of an interferometer acting in the farfield regime of single molecule diffraction, the interaction between a diffractive element and neutral and polar molecules are investigated. This interaction rises from the potential a particle feels while it passes a small aperture, such as a grating, of finite thickness. Further the molecular scattering cross section was investigated in this setup and evaluated using different approaches. Also interferometric studies of the effect of electrons deposited onto the grating bars were carried out.



# Table of contents

Zusammenfassung	v
Abstract	v
1 Introduction	9
2 Theory	11
2.1 Basics of quantum mechanics	11
2.2 Diffraction theory	13
2.2.1 Conditions on matter waves	13
2.2.1 Grating diffraction	15
2.3 Farfield diffraction of molecules	19
2.3.1 Van der Waals forces	20
2.3.2 Dipole forces	21
2.3.3 Rotation of the diffracting element	23
3 Experimental setup	27
3.1 Vacuum	27
3.2 Source	29
3.3 Beam preparation	33
3.3.1 Velocity selection	34
3.4 Diffracting element	35
3.5 Detection	37
3.6 Molecules	39
3.6.1 Phthalocyanine	40
3.6.2 Rhodamine 6G	41
3.6.3 Rhodamine B	43
4 Experimental data	45
4.1 Polar particles	45
4.2 Discussion of <i>van der Waals</i> interactions	53
4.2.1 Charges on the grating	54
4.3 Pressure dependent diffraction	57

5	Outlook	60
5.1	Atomically thin diffraction gratings: graphene	60
5.2	Light gratings for a new type of diffraction	61
6	Conclusion	62
7	Appendix	63
7.1	Technical drawings	63
8	Bibliography	67
9	Acknowledgements	74
	Curriculum vitae	75

# 1 Introduction

In the early beginnings of quantum mechanics physicists had different views of breakthrough ideas. One of those was the thesis of *Louis de Broglie*, in which he described the electron as wave and a particle [1]. The noble laureate *Max von Laue* said about it that ‘If that turns out to be true, I’ll quit physics.’ In 1927, just a few years after that, *Clinton Davisson* and *Lester Germer* provided the experimental proof [2], that *de Broglie’s* assumption was correct. Today we know that not only electrons, but also other individual physical entities, can behave like waves. This is uncommon in daily life and therefore gives an interesting extension to the insight of how our world seems to work. Applying *de Broglie’s* hypothesis leads us to assigning wavelike properties to each piece of matter.

After *Davisson* and *Germer* successful experiments many studies were performed to demonstrate the matter-wave duality for instance for neutrons [3,4,5,6], atoms [7,8,9] or molecules [10,11,12,13]. The fact that we experience ourselves in a classical world leads us to the question if there is a border that separates classical physics from quantum phenomena. We ask under which conditions such quantum effects can be extended to massive and complex macroscopic particles [14]. One approach to this question is to perform interferometric experiments on molecules, pushing their mass to the experimental limit. Different models describe the interface between an isolated system and the measuring apparatus, that couples to classical output. Those are expected to be probed with molecular quantum interference soon, such as continuous spontaneous localization theories [15,16]. So far the particle with the highest mass that shows wave nature is a modified tetraphenylporphyrine with 810 atoms and about 10.000 atomic mass units. This was demonstrated at the *Kapiza-Dirac-Talbot-Lau-Interferometer* at the Faculty of Physics at the University of Vienna [17].

With diffraction experiments, we can visualize the wave nature of complex molecules and perform measurements on internal molecular properties [18,19]. Interactions between the molecule and the nanomechanical diffraction mask affect the interference pattern and can be studied this way. This is an experimentally challenging task, because most of the time several different effects may come into play. For molecules propagating through a mechanical grating *van der Waals* forces as well as a polar

structure of the molecule must be considered for instance. Detailed theories have been developed and have to be fit to the experimental data. Molecular diffraction is a good tool to test these models as well as it enables us to study forces acting on the nanoscale.

## 2 Theory

### 2.1 Basics of quantum mechanics

#### Quantization of energy

At the beginning of the 20<sup>th</sup> century *Max Planck* followed from investigations of blackbody radiation that the energy  $E$  has to be quantized in terms of the wavelength  $\lambda$ , the speed of light  $c$  and a constant  $h$  [20].

$$E = \frac{hc}{\lambda} \quad \text{with } h = 6.62606957 \cdot 10^{-34} \text{ J s} \quad (2.1)$$

This was the only way to combine the theory of *Rayleigh-Jeans* with the one of *Wien*. Each were able to explain only a part of the experiments performed on blackbody radiation [21]. Formula (2.1) implies, that the energy of a physical process can only be described in discrete multiples of a smallest portion, the *Planck's constant*  $h$ . It defines a size of the 'grain of energy' and causes the origin of quantum effects.

#### Wave-particle duality: matter-waves

In quantum physics the physically sensible description of a process depends on the situation. A photon, for instance, can be described as a wave or a particle respectively [22]. In the same way each particle can behave like a wave under special conditions. This is known as matter-wave to which a certain wavelength is ascribed, defined by its momentum.

$$\lambda_{dB} = \frac{h}{p} = \frac{h}{m \cdot v} \quad (2.2)$$

This *de Broglie* wavelength  $\lambda_{dB}$  is dependent of the mass  $m$  of the particle, its velocity  $v$  and *Planck's constant*  $h$ . For matter-wave optics this means that any object of a certain mass traveling at a finite speed will show wave effects like diffraction or interference. An issue in any matter wave experiment is to get a preferably monochromatic beam

of molecules in the right range of wavelength. The correct quantum mechanical description of such a beam consisting of isolated particles is a coherent sum over wave packets. The wave packets group velocity is the one leading to a specific *de Broglie* wavelength of the particle.

From equation (2.2) we see that the mass and the velocity of a molecule have got the same effect on the wavelength. Thus, we are able to investigate relatively light but fast moving molecules in the same way as massive molecules that move slowly. Thus, it is experimentally more challenging to investigate heavy molecules due to the need of molecules in the gas phase moving at slow velocities.

## Uncertainty relations

Quantum formalism [23] as well as experimental results [24] show, that the knowledge of two variables describing a physical process is limited. The best known example for this rule is that the momentum  $p$  and the position  $x$  of a particle obey the following relation

$$\sigma_x \cdot \sigma_p \geq \frac{\hbar}{2}, \quad (2.3)$$

with  $\sigma$  being the standard deviation of the experimentally measured outcome.

Not only observables like position and momentum, but any two complementary variables in quantum mechanics such as energy and time, have to obey an uncertainty relation. This depends on the outcome of the commutator of the observables, which is denoted as  $[A, B] = AB - BA$ . According to this, a general form of (2.3) is denoted as

$$\Delta A \cdot \Delta B \geq \frac{1}{2} | \langle [A, B] \rangle |, \quad (2.4)$$

where the deviation of an observable  $\Delta A = \sqrt{\langle A^2 \rangle - \langle A \rangle^2}$  is defined by the expectation value of the normalized wave function  $\langle A \rangle_\psi = \langle \psi | A | \psi \rangle$ . The definition of (2.3) is generally true for a wave packet of a Gaussian form. Collimating a molecular beam by using slits it has been shown experimentally [25] that the uncertainty principle can be written as  $\Delta x \cdot \Delta p = 0.89h$ .

## 2.2 Diffraction theory

### 2.2.1 Conditions on matter waves

Matter wave interference is a possibility to detect and prove the quantum nature of molecules. It is only observable if the particle can be described by a wave and therefore differs from a classical scattering process. While a matter-wave can pass many slits of a diffraction grating at the same time, a classical particle just passes one. In order to show the interference of the matter-wave behind the grating it has to illuminate many grating slits in a coherent way.

### Coherence

In physics the term *coherence* is associated to the property of a wave to have a constant phase over a certain time and region in space. Given a one-dimensional wave in vacuum  $\psi(x, t) = \psi_0 \cdot e^{i(k \cdot x - \omega \cdot t)}$  its phase can be described by the exponent  $\phi = (k \cdot x - \omega \cdot t)$ . It essentially describes each part of a period of the length  $\lambda = \frac{2 \cdot \pi}{k}$  with respect to a reference point in space and time.

Any wave packet can be described as the sum of waves with a distribution of different wavelengths  $\lambda \pm \Delta\lambda$ . Within a region of space and time, where their phases do not differ by more than  $\Delta\phi \leq \frac{\lambda}{2}$  constructive interference is possible. These are called coherence time  $\tau_c$ , or coherence length  $l_c$  respectively:

$$l_c = \tau_c \approx \frac{\lambda^2}{\Delta\lambda}, \quad (2.5)$$

This relation is mathematically expressed by the theorem of *N. Wiener* and *A. Chintschin* [27,28], which states that the coherence length can be described as the fourier transform of of the spectral width of the source.

On the other hand, an argument of *P. van Cittert* and *F. Zernike* may be used to describe [29, 30] the part of the coherence transverse to the propagation of the wave. The spatial coherence of a distant incoherent source is therefore characterized by the fourier transform of the intensity at the source.

This relation can be simplified to

$$l_t = \frac{\lambda \cdot L_1}{\Delta s}, \quad (2.6)$$

with  $\lambda$  being the wavelength of the propagating wave,  $L_1$  the distance between source and illuminated object and the source size  $\Delta s$ .

A plane wave is coherent everywhere transverse to its direction of propagation. Working with spherical waves starting at a large distance the wavefront will become flat enough, such that a diffracting aperture can be coherently illuminated.

## Decoherence

The term *decoherence* is ascribed to mechanisms causing a system to lose its properties of wave interference. Often the word *dephasing* is also used in this context. Therefore, in the following a short definition of both should be given to clarify the terminology in this work. Both mechanisms act on the propagating wave in a way that disturbs or even destroys the recorded interference in the end. Dephasing in this work will be used for actions of parts of the experimental setup that slow down or accelerate parts of the wavefront. In this sense it is possible that between two spatially separated beams the ability to interfere is destroyed. If it is the case that the whole wave front undergoes dephasing the quality of interference should be kept. With a pure dephasing mechanism no 'which way' information that would lead to decoherence can be gained.

Due to the interaction of the experimental surrounding and the investigated object, both are entangled [32,33]. This entanglement offers the possibility to gain knowledge about the objects properties by the entangling parties. If the rate at which this happens becomes too high, the quantum state can not be distilled any more. It irreversibly destroys the possibility of self interference, for instance, at a grating. This mechanism is usually called decoherence.

## 2.2.1 Grating diffraction

In order to describe the diffraction of waves at an arbitrary aperture we follow the theory developed by *Kirchhoff* and *Fresnel* (such as described in [31]). Its aim is to get the intensity distribution of a wave on a detector screen  $S$  after passing an arbitrary aperture  $P$ . The graphical representation of that situation is shown in figure 2.2. We investigate the situation of an arbitrary disturbance in space, as shown in figure 2.1, first.

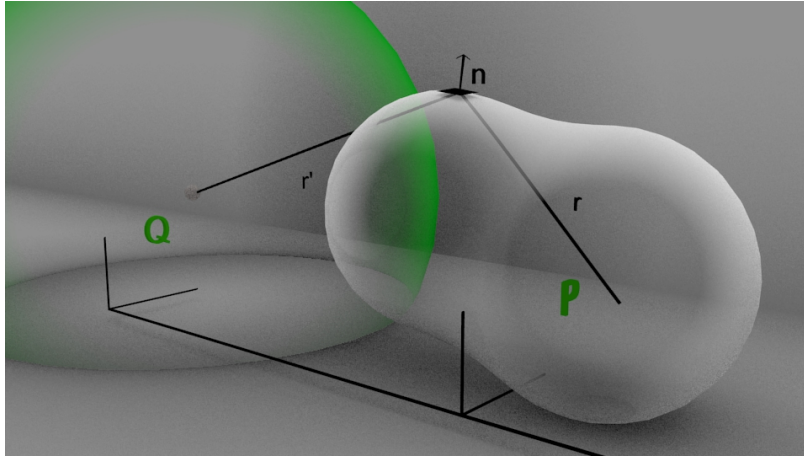


**Figure 2.1** Starting from a source  $Q$  a spherical symmetric wave (green sphere) reaches a region (white surface) around a point of disturbance  $P$ . The vector  $n$  denotes the normal vector on the surface element  $dS$ , while  $r$  and  $r'$  are the vectors from the point  $P$  and  $Q$  to the surface element, respectively.

We start from the scalar wave equation as known from electrodynamics. For the electric field we write

$$\nabla^2 E = \frac{1}{c^2} \frac{\delta^2 E}{\delta t^2}. \quad (2.7)$$

Assuming monochromatic waves we can insert the *ansatz*  $E = \mathcal{E} \cdot e^{-ikct}$  into (2.7), where  $\mathcal{E} = \mathcal{E}(r')$  denotes the spatial part of the complex amplitude at the disturbance. This leads to the *Helmholtz* equation

$$\nabla^2 \mathcal{E} + k^2 \mathcal{E} = 0, \quad (2.8)$$

where  $k = \frac{2\pi}{\lambda}$  denotes the wave vector of the propagating wave. This equation can be solved on a closed surface  $S$  around an arbitrary point  $P$  using *Greens* theorem. After a bit of calculation one ends up with the formula

$$\mathcal{E}_P = \frac{1}{4\pi} \left\{ \oint_S \frac{e^{ikr}}{r} \nabla \mathcal{E} dS - \oint_S \mathcal{E} \nabla \left( \frac{e^{ikr}}{r} \right) dS \right\}, \quad (2.9)$$

often stated as *Kirchhoff integral theorem*. Now the geometry of the emitted wave comes into play, where we assume the general case of a spherically symmetric wave  $E(r', t) = \frac{\mathcal{E}_0}{r'} e^{i(kr' - \omega t)}$  with  $\mathcal{E}(r') = \frac{\mathcal{E}_0}{r'} e^{ikr'}$  emitted from a point like source  $Q$ . Again after some calculation and the assumption, that  $r' \gg \lambda$  as well as  $r \gg \lambda$ , (2.9) changes to

$$\mathcal{E}_P = -\frac{\mathcal{E}_0 i}{\lambda} \oint_S \frac{e^{ik(r+r')}}{rr'} \left[ \frac{\cos(n, \hat{r}') + \cos(n, \hat{r})}{2} \right] dS, \quad (2.10)$$

known as *Kirchhoff-Fresnel's* diffraction formula. The term inside the rectangular brackets is often referred to as the slope factor. It tends to 1 for large distances between the components  $Q$ ,  $P$  and  $S$  or a small diffracting aperture. This case is called farfield regime of diffraction or *Fraunhofer* approximation.

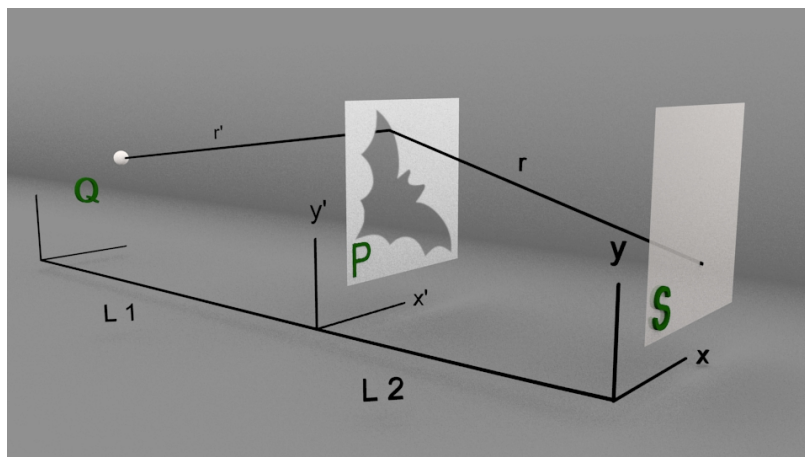


**Figure 2.2** Starting from a source  $Q$  a wave passes an aperture  $P$  ending at the detector screen  $S$ .

Further simplifications are possible if we take into account the special form of our diffracting object. We send the surface over which we integrate in (2.10) to infinity, so that the only surface that remains is the transmitting part of our aperture  $P$ .

This situation is shown in figure 2.2. The denominator  $rr'$  is approximated with the two lengths  $L_1$  and  $L_2$ , whereas the encounter has to be treated different. The information about the phase is imprinted in the exponent and with it the ability to interfere. This makes it necessary to expand the distance  $r = \sqrt{(L_2)^2 + (x - x')^2 + (y - y')^2}$ . Thus, we get the field at the screen  $S$

$$E_S(x, y) = \frac{e^{ikL_2}}{i\lambda L_2} \int \int_A t(x', y') \cdot e^{\frac{ik}{L_1 L_2} [(x'-x)^2 + (y'-y)^2]} dx dy, \quad (2.11)$$

with  $t(x', y')$  being a function describing the intensity of the spherical wave at the aperture. If the characteristic opening of the aperture and the term  $\frac{1}{\lambda}(x'^2 + y'^2)$  are much smaller than  $L_2$ , quadratic terms in the integral dependent of  $x$  or  $y$  can be neglected, known as *Talbot* condition and the expression further simplifies to

$$E_S(x, y) = \frac{e^{ikL_2}}{i\lambda L_2} \cdot e^{\frac{i\pi}{\lambda L_2}(x^2 + y^2)} \int \int_A t(x', y') \cdot e^{\frac{ik}{L_2}(x'x + y'y)} dx dy. \quad (2.12)$$

The definition of the variables

$$|\vec{s}| = \sqrt{x^2 + y^2} \quad , \quad |\vec{p}| = \sqrt{x'^2 + y'^2}$$

$$\text{and } \vec{K} = \vec{p} \frac{k_0}{L_2}$$

offers the possibility to draw a connection between the approximation of *Fraunhofer* and the Fourier transform of the aperture, with  $\mathcal{A}$  collecting the prefactors in front of the integral

$$E_P(x, y) = \mathcal{A} \int \int_A t(x', y') \cdot e^{i\vec{K}\vec{s}} dx dy. \quad (2.13)$$

For a periodical grating, there is a second approach to the *Fraunhofer* approximation, that is more practical in daily work. In the case of such a periodical structure one starts from *Huygens* principle, which states, that each illuminated point in an aperture itself acts as a source of a spherical wave. In a grating, each grating slit can thus be treated as point like source emitting into the whole space. In general, two waves

interfere constructively for angles such that the path difference  $\Delta s$  equals integer multiples of the wavelength (see figure 2.3). Summing up all coherently illuminated slits in a grating leads then to the equation

$$I(\Theta) = I_0 \cdot \left( \frac{\sin \beta}{\beta} \right)^2 \left( \frac{\sin N \alpha}{\sin \alpha} \right)^2, \quad (2.14)$$

$$\text{with } \beta = \frac{kb}{2} \sin \Theta \text{ and } \alpha = \frac{kd}{2} \sin \Theta,$$

where  $\Theta$  is defined as shown in figure 2.3.

The parameters are the  $k$  vector of the molecular wave, the grating period  $d$  and the width of a single slit  $b$ . This formula shows that the single slit is responsible for the envelope of the pattern. The grating with its  $N$  slits, defines the position of the interference maxima. It can be shown that formula (2.14) has maxima for  $\alpha = 2n\pi$ . This leads to a formula for estimating the angle to the  $n$ -th interference maximum at the detector screen.

$$n \cdot \lambda = d \cdot \sin(\theta). \quad (2.15)$$

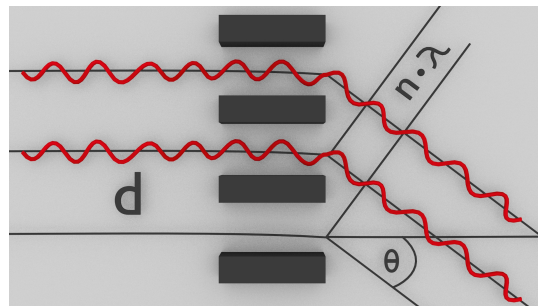


**Figure 2.3** Condition for constructive interference after a grating described by (2.15): The path difference between two waves evolving from different slits has to equal multiples of the wavelength.

The formulas in this chapter describe a diffraction experiment in the farfield regime to a first approximation. To describe the outcome of a real setup further terms have to be added. These will take into account specific interactions of the aperture with the

traversing particles. Some examples, which will be treated in the next chapters are *van der Waals* or dipole interactions.

### 2.3 Farfield diffraction of molecules

In the previous chapter we derived expressions that were initially found with the intention to describe the behavior of electromagnetic waves. Based on the *Schrödinger equation* [26]

$$i\hbar\frac{\delta}{\delta t}\psi(r,t) = \left(-\frac{\hbar^2}{2m}\nabla^2 + V(r,t)\right)\psi(r,t), \quad (2.16)$$

one can define a dispersion relation for the wave-vector of matter waves [34]

$$k^2 = 2m\frac{(E - V(r))}{\hbar^2}, \quad (2.17)$$

where  $E$  denotes the energy eigenvalues and  $V$  the potential for a particle of mass  $m$ . Thus, the analogy between electromagnetic waves and matter waves can be used to investigate many wave like effects. Electron diffraction and atom interferometry have been successfully studied [35, 36, 37] and an expansion of these concepts to molecular matter waves is a logical next step. From the dispersion relation (2.17) we can already estimate that the description of molecules in an interferometric setup is a bit more complicated, than electromagnetic waves that travel through a grating. Usually molecules have a huge number of degrees of freedom due to their complex structure. Those are able to couple to the surrounding, leading to additional decoherence channels for the matter wave [38]. The experimental challenge is to shield a molecular quantum system in a way that the wave nature can be evoked and preserved.

Working at low pressures in a vacuum system, which will be specified in more detail in the experimental part of this work, provides a good base for diffraction experiments. It guarantees that the molecules are not disturbed by collisions with for instance nitrogen or oxygen molecules. Once this condition is met effects of the grating on the molecular beam can be studied. Due to the fact that each molecule passes the edge of the aperture in a finite distance, it will feel the potential from the grating bars [39, 40, 41, 42].

### 2.3.1 Van der Waals forces

For an understanding of *van der Waals* forces, first described by *Fritz London* [43], we consider the situation of a neutral particle  $A$  in an external electric field  $E$ . This will induce a dipole moment  $p_A^{ind}$  proportional to the particles polarizability  $\alpha$ :

$$p_A^{ind} = \alpha_A \cdot E \quad (2.18)$$

and will therefore feel a dipole potential

$$V_{pot} = -p_A^{ind} \cdot E = -\alpha_A E^2. \quad (2.19)$$

This is also the case for a particle feeling the electrical field of an ion or a second polar particle. In molecular matter wave experiments the situation is a bit different. Our experiments uses neutral particles. Although the mean dipole moment of a neutral molecule  $\langle p_A \rangle$  is zero, there are always fluctuations in the charge distribution forming a short-term dipole moment  $p_A$  at a femtosecond time scale. The electrical field of this dipole is strong enough to influence another neutral particle  $B$ , which will polarize, leading to the corresponding back action. Thus the mean dipole moment will no longer be zero. It gives rise to a potential, depending on the polarizabilities and the distance  $r$  between both opponents [44]

$$V_{pot}(r) = -C_{disp} \frac{\alpha_A \cdot \alpha_B}{r^6}, \quad (2.20)$$

known as the *van der Waals* potential. Its strength is proportional to a constant  $C_{disp}$  that will be adopted to our situation by  $C_3$  later. The dependencde on the sixth power of the distance  $r$  rises from the geometry of two point dipoles, each with a power law of  $1/r^3$ . However, our experiment is a bit different. We have to adopt the formulas for the situation of a particle traveling along a plane of finite length. The correct description of this geometry requires a detailed theory that has been developed by *Prof. Dr. Stefan Scheel* and *Dipl.-Phys. Johannes Fiedler* at the University of Rostock. Here we focus on a qualitative description, which considers the molecule close to an infinite wall. In such a case, the *van der Waals* potential is described by

$$V_{pot}(r) = -\frac{C_3}{r^3}. \quad (2.21)$$

with

$$C_3 = \frac{\hbar}{4\pi} \int_0^\infty \alpha(i\omega)g(i\omega)d\omega. \quad (2.22)$$

It is determined by the frequency dependent polarizability  $\alpha(i\omega)$  of the particle and the dielectric function  $g(i\omega) = (\epsilon(i\omega) - 1)/(\epsilon(i\omega) + 1)$  of the polarizable wall, integrating over all frequencies  $\omega$  [45,46].

Describing a molecule interaction with the wall of the grating slit raises the question whether the interaction localizes the particle and therefore destroys the interference contrast. Experiments have shown that this is actually true if the interaction opens an additional decoherence channel [55]. If that is not the case the delocalization of the molecule over several grating bars is sufficient to overcome this problem. In a quantum mechanical framework each molecule, behaving like a wave, is delocalized over all coherently illuminated grating bars. Thus, the molecule feels the potential of all grating slits at the same time. During the transit through the grating the phase  $e^{i\phi}$  of the matter wave is changed. This additional phase results in an effective reduction of the gratings slit width. Thus, in our diffraction formalism the *van der Waals* potential is included into the transmission function via

$$t'(x) = t(x) \cdot \exp\left(-\frac{i}{\hbar} \int_0^\tau V_{pot}(x) \frac{dz}{v}\right), \quad (2.23)$$

where  $t(x)$  is the geometrical binary transmission function and  $V_{pot}(x)$  denotes the potential as described in (2.21) reduced to one dimension. The integration is performed over the time  $\tau$  the particle with velocity  $v$  spends in the potential.

### 2.3.2 Dipole forces

Permanent electric dipole moments are determined by the chemical structure of the particle. They arise from a difference of electronegativities of atoms in a molecule. This dipole  $p_A$  also induces a dipole moment  $p_B$  in a dielectric surface near by, which results in an attractive force. Additionally there is again the effect of the induced

dipole moment of fluctuating charges in the polarizable molecule. Due to the the fixed orientation of the permanent dipole in the molecular frame the interaction in general also depends on the orientation of the molecule to the surface. The whole interaction is described by [44,45]

$$V_{pot}(r) = - [C_{ind} + C_{orient} + C_{disp}] / r^3 \quad (2.24)$$

The last term of (2.24) is already known from pure *van der Waals* interactions of neutral non-polar particles (2.22).

The second term in the brackets represents the angle averaged orientation dependency of the dipole relative to the second one. For the situation of our experiment there is just one polar opponent, namely the molecule. The grating wall is expected to have no permanent dipole moment. On short timescales, an angular dependency of the permanent dipole moment might still be relevant. Calculations (ChemBioOffice-software) for the molecular moments of inertia  $\xi$  and the relation  $kT = \frac{1}{2} \cdot \xi \cdot (2\pi\nu)^2$  show that mean rotational frequencies  $\nu$  of the investigated molecules such as rhodamin B are in the range of  $\nu \approx 80$  GHz. In a two dimensional simplified picture this frequency corresponds to about 3 nm distance, a molecule at a speed of 250 m/s travels. For diffractive objects that are thicker than that, it is reasonable to take the angle averaged potential for the effective interaction between the grating wall and the molecule.

The first parameter in (2.24) describes the influence of the static dipole moment of the particle onto the wall. The effective angle averaged potential for our experiment thus reads as [44]

$$V_{pot}(r) = - \left[ \frac{p_A^2}{4\pi\epsilon_0} \cdot \frac{\epsilon_B - 1}{\epsilon_B + 1} + C_3 \right] / r^3, \quad (2.25)$$

with  $\epsilon_B$  being the relative permittivity at  $\omega = 0$  of the grating wall.

The fact that the strength of the interaction is frequency-dependent and hence influenced by the frequencies of the molecular transitions introduces retarded field effects. Thus we can ignore these retardation effects only for short distances  $x \ll c/\omega$ , where

$c$  denotes the speed of light. For distances larger than that the potential changes to a  $1/r^4$  dependency corresponding to the arrival and the departure of a molecule from the grating. A detailed description of this effect is known as *Casimir* forces [47,48].

### 2.3.3 Rotation of the diffracting element

As the interference pattern depends on the geometrical properties of the absorptive diffraction grating one can modify it in a controlled way. This can be achieved by a rotation of the grating with respect to the molecular beam [35,49]. The resulting effect on the molecular beam is twofold. On the one hand, the rotation leads to an effective reduction of the projected distance between the grating bars. According to equation (2.15) the angle of diffraction for a fixed wavelength will increase and the maxima are separated further from each other at the detection screen. This results in a better resolution of the interferogram at the detector.

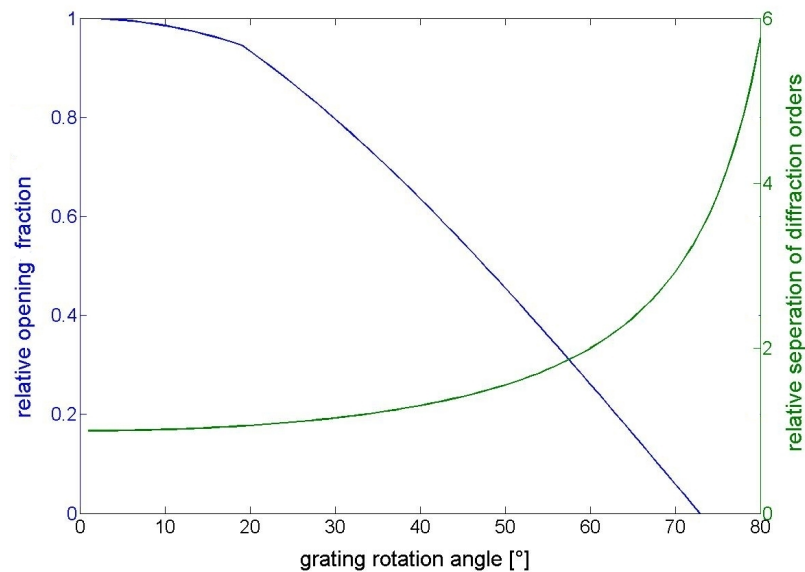


**Figure 2.4** The geometrical effect of rotating the grating with respect to the molecular beam shown for a grating with a thickness of  $t = 20$  nm and an initial opening fraction  $f = 0.68$ . As the angle of rotation increases the relative opening fraction and thus the transmission through the grating will decrease described by (2.26) (blue curve). At the same time the angle of diffraction will increase due to a shrinking of the effective grating periodicity. The effect on the first diffraction order relative to the zeroth order is shown (green curve).

A bigger angle of diffraction may offer also the possibility to test molecules with a higher mass. This effect is shown in the green curve of figure 2.4.

Starting with a molecule of mass  $M$  a rotation of the grating by an angle  $\alpha = 60^\circ$  for instance leads to a diffraction angle, that is twice as big. This enables to diffract molecules with a mass of  $2M$  without losing resolution.

On the other hand, the open fraction of a rotated grating will decrease. This is a purely classical effect and leads to a signal reduction for a grating with a certain thickness. This effect has to be studied carefully because of the gratings geometry. It can be different for each grating due to the fabrication process, which can be done for instance by focused ion beam milling. This induces a wedge angle that differs from grating to grating. In the rotated case the molecular beam is then more affected by the edges of the slits, than by the walls, sketched in figure 2.5.

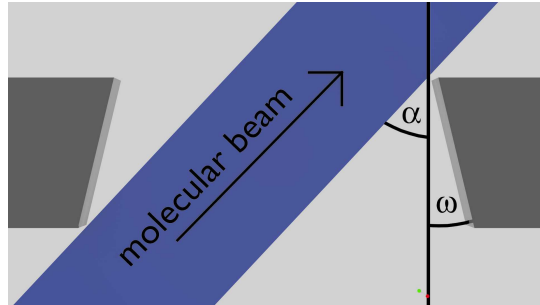


**Figure 2.5** The effect on the molecular beam by the rotation of the grating. The angles denote the wedge angle  $\omega$  rising from the production process and the angle of rotation  $\alpha$  with respect to the starting position orthogonal to the beam.

Because of this special geometry the mathematical description of the open fraction  $f(\alpha)$  under rotation has to be split. The first part describes rotation angles  $\alpha$  between zero degree and the wedge angle  $w$ .

$$f(\alpha_1 \leq w) = o \cdot \cos(\alpha) \quad (2.26)$$

The second part describes the situation from the wedge angle on to the point, where the geometric reduction of the initial opening  $o$  tends to zero

$$f(\alpha_2 \geq w) = o \cdot \cos(\alpha) - t \frac{\cos(\frac{\pi}{2} - \alpha + w)}{\cos(w)},$$

where  $t$  denotes the thickness of the grating. From that it is clear, that the thickness of the grating influences the signal intensity behind a rotated grating. A sketch of this is shown in 2.6 while quantitative numbers are shown in 2.7. It is therefore interesting to choose gratings that are as thin as possible.

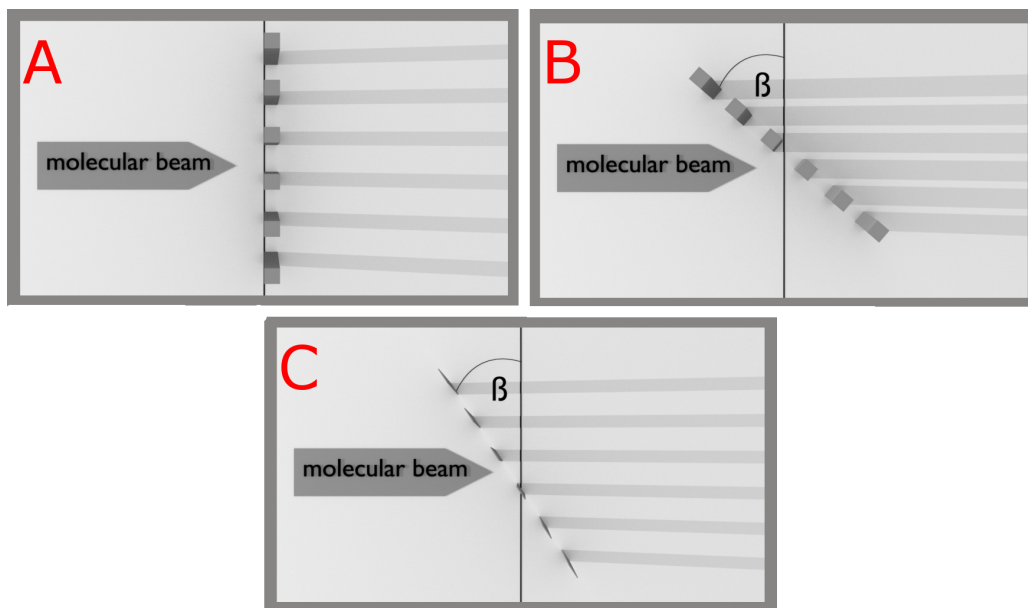


**Figure 2.6** Classical signal reduction behind a (A) nonrotated thick grating, (B) a rotated thick grating and a (C) rotated thin grating.

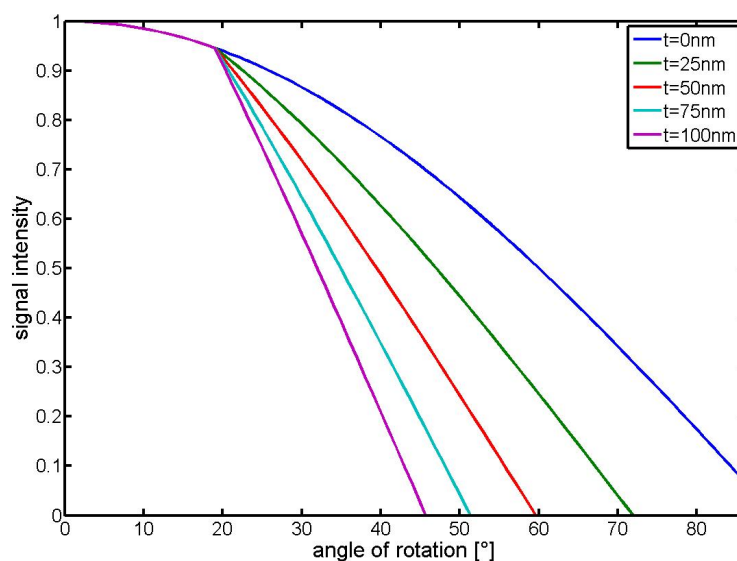


**Figure 2.7** Comparison of the signal reduction behind a grating with an initial open fraction of  $f = 0.68$  and a wedge angle of  $w = 19^\circ$  for different thicknesses  $t$ . Up to the wedge angle the reduction of the signal shows a cosoidal behaviour while for higher angles the thickness of the grating reduces it as well.

The reduction in slit width offers the possibility to alter the *van der Waals* potential between grating walls and molecules, as shown in figure 2.8. As the grating is rotated, more and more particles are effected by steeper parts of the potential. The geometric slit width and the effective reduction due to this potential lead to an effective opening

fraction of the grating, from which the *Van der Waals* interaction can be followed (see 2.23). Similar to a smaller slit, the rotated slit increases the population of the maxima of higher order interference fringes. There exists a rotation angle, where molecules that would geometrically pass the grating will nevertheless not arrive at the detection plate. This occurs due to the influence of the *Van der Waals* interaction. This may be useful estimating offsets in the model of the interaction between grating wall and molecule. Unfortunately this point is not reached in the experiment so far due to the fact, that the support structure of most of the gratings blocks the molecular beam before reaching this angle.

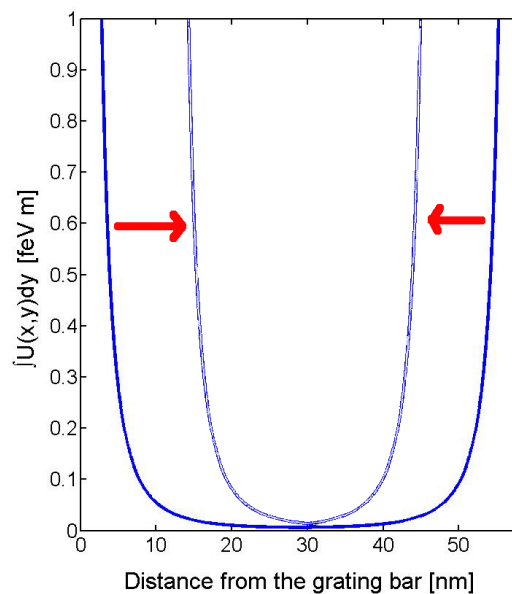


**Figure 2.8** Modification of the van der Waals potential due to the decrease of the opening fraction of the diffraction grating. The second grating bar is situated 60 nm from the first one.

## 3 Experimental setup

An overview of the experiment is sketched in figure 3.1 whereas the laboratory realization is shown in figure 3.2.

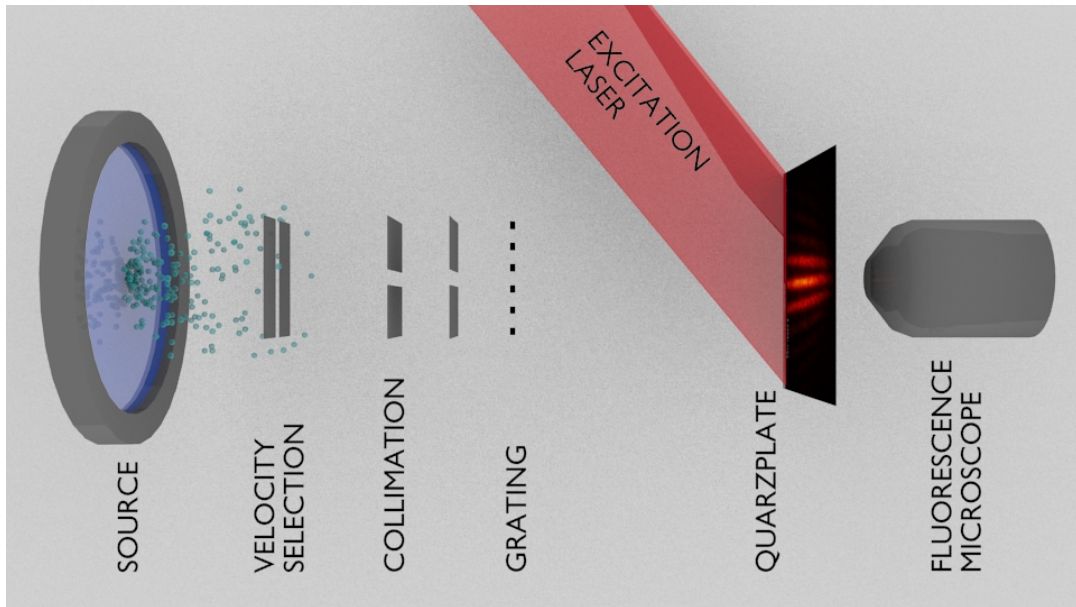


**Figure 3.1** Sketch of the molecular diffraction experiment. The main parts described in the following sections are the source (described in section 3.2), the beam preparation (section 3.3) consisting of collimation and velocity selection slits, the grating (section 3.4) and the detection (section 3.5) consisting of the excitation laser, the quartz plate and the fluorescence microscope.

### 3.1 Vacuum

We have to guarantee that the molecules that traverse the experiment will end at the detector undisturbed by any rest gas particle. For our setup it is geometrically necessary to ensure a minimum length of about two meters of free flight for a molecule to prepare coherence with a point like source on the one hand and to be able to collect the signal of the farfield interference fringes on the other hand. To fulfill this condition it is needed to work with evacuated chambers, in which the free flight of a molecule can be achieved. For phthalocyanine molecules those should be operated at a pressure below  $2 \times 10^{-7}$  mbar for a good quality of the interference pattern. The mean free path of our molecules would already be long enough with the setup operated in the  $1 \times 10^{-6}$  mbar regime, as can be seen in figure 3.3 but the experiment is usually run at the lowest possible pressure that can be reached with our machine.

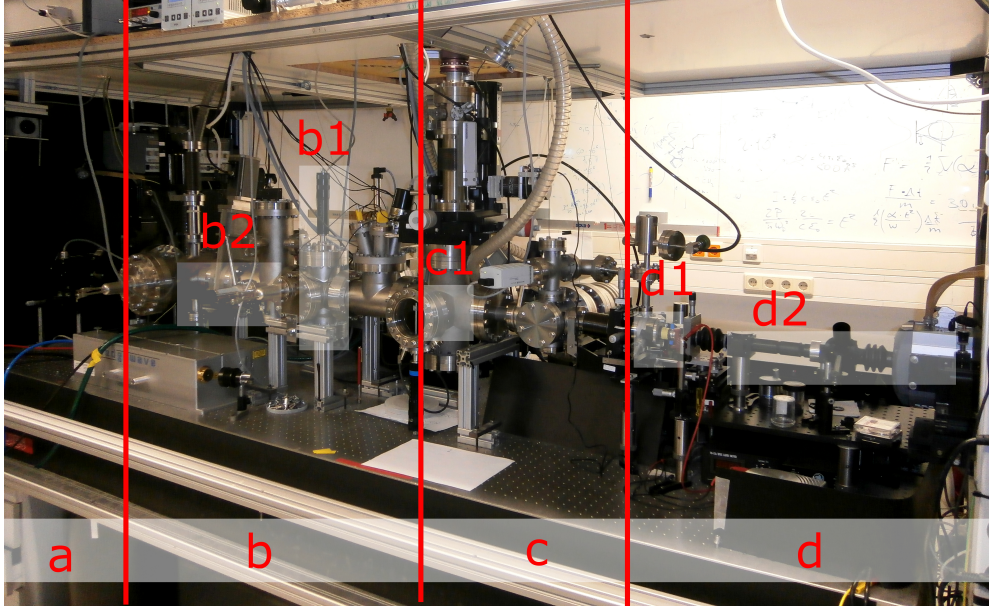


**Figure 3.2** Realization of the molecular farfield interferometer. The sections are the source (a), the beam preparation (b) with the velocity selection (b1) and a  $1\ \mu\text{m}$  collimation slit (b2), the grating (c1) and the detection (d) with the quartz plate (d1) and the fluorescence microscope (d2).

This is mostly limited by the fact, that we have to break the vacuum of parts of the vacuum chamber from time to time to refill the source, for instance. The molecules would already reach our detection plate at such high pressures, but there would be a bad ratio of signal to noise because a hit from a rest-gas atom can still disturb our molecules or even kick it out of the detector range.

At this point we have to keep in mind, that the requirements on the vacuum also depend on the specific molecule used and its properties. The vapor pressure of the molecule during the evaporation process may influence the quality of the vacuum in the source chamber. The scattering cross section of the molecule will influence the length of its mean free path within the vacuum chamber.

In our experiment a backing pump reaches about  $10^{-1}$  mbar to  $10^{-2}$  mbar. After that four molecular turbo pumps get each part of the whole vacuum chamber (as defined in figures 3.1 and 3.2) to a pressure between  $8 \times 10^{-8}$  and  $9 \times 10^{-9}$  mbar.

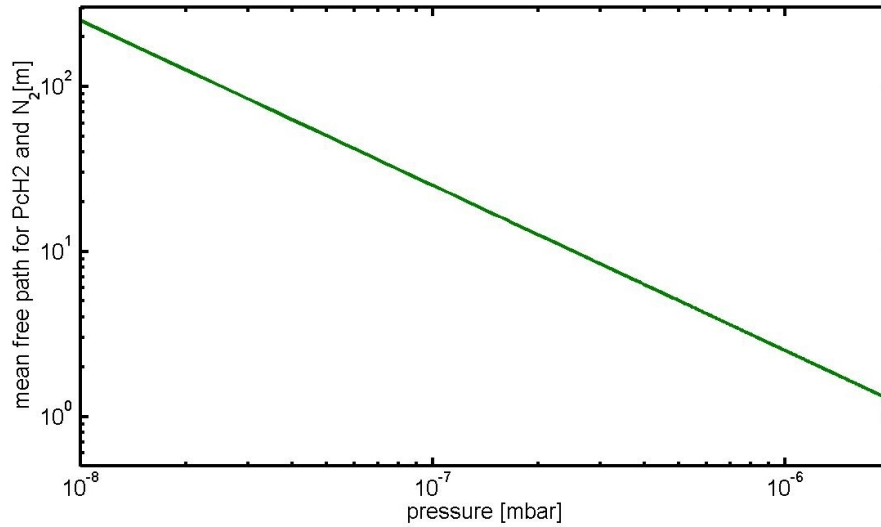


**Figure 3.3** Double logarithmic plot of the mean free path for phthalocyanine and  $N_2$ . Experiments show that the border of a molecular free flight through the whole vacuum chamber is at a pressure of about  $7 \cdot 10^{-7}$  mbar.

## 3.2 Source

Molecular diffraction experiments impose several requirements on the source. It has to offer transverse coherence in order to illuminate a number of slits of the diffracting grating, so that quantum interference is possible. We meet these conditions by a thermal micro focus collimated source that emits molecules in any direction of half space, indicated with the blue dots in figure 3.1. Due to trigonometrical considerations we put the source roughly one and a half meter away from the diffracting grating. This guarantees, that slits are able to sort out just those molecules, that come from a angle of less than five micro radians for a source spot size smaller than  $5 \mu\text{m}$ . The real size of our source is usually smaller. It uses a cw diode laser centered at  $421 \text{ nm}$  wavelength with  $62 \text{ mW}$  power that gets focused by an objective down to about  $1.6 \mu\text{m}$  full with half maximum of the Gaussian profile (see figure 3.4). The focus point is set to the inside of a vacuum window that is coated with the molecular species we want to investigate.

In a simplified picture the molecules get heated at the focus point of the laser and go into the gas phase. To constantly get a fresh spot of molecules the vacuum window has to be moved in order to end up with a useful signal. Various parameters influence the quality of the signal:

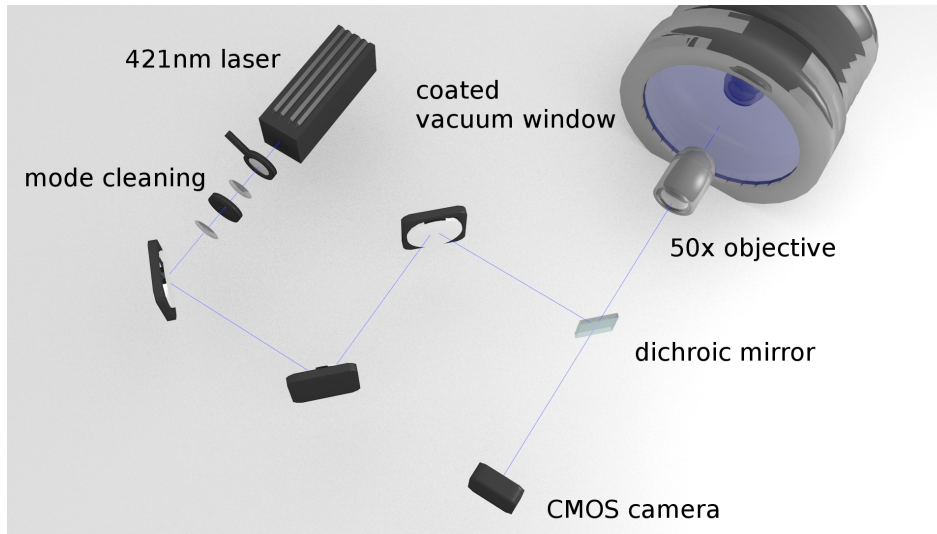


**Figure 3.4** Schematic drawing of the source setup. A Gaussian laser profile of a 62 mW cw-laser centered 421 nm gets selected by a mode cleaning stage consisting of two lenses and a pinhole. After that it is focused through an objective onto the inside of a coated vacuum window. The fluorescent light from the evaporated molecules is collected with a CMOS camera after a dichroic mirror.

- *Molecules:* The molecules used in our experiments vary in their physical properties as we will see in section 3.6. The most important parameter is the temperature of sublimation. In the source we have to overcome this temperature twice. First when we coat the molecules onto our vacuum window and second in the beam source of the interferometer. The coating happens in a separated setup. The window is then transferred to the diffraction setup. There the molecules are evaporated by the focused laser beam, which imprints a *Maxwell-Boltzmann* distribution of velocities onto the molecular beam. This distribution depends on the sublimation temperature of the molecule (see figure 3.8 for the experimental observation of this effect).
- *Scanning speed and laser spot size:* In order to achieve good transverse coherence the point of evaporation, should be as small as possible. There are two different approaches that lead to similar results. The first one is to scan the vacuum stage slowly to continuously expose fresh areas of molecular layers to the laser beam. That leads to a constant evaporation of molecules within the area of the Gaussian laser beam that is above an effective threshold with its intensity. Once the molecules absorbed enough energy, they will evaporate. To achieve a small desorption area, one would have to optimize the laser intensity such, that the maximum of the

Gaussian beam is just above this threshold. This is hard to do for each molecule and would need further optimization [50].

Here we scan as fast as possible (1 m/s) with the highest laser power we can achieve (3 MW/cm<sup>2</sup>). This guarantees a Gaussian laser beam with a steep flank, which means that the region within which it crosses the evaporation threshold is small. Note that this is only true in the direction of the stage movement. Orthogonal to it we still have the distance between both Gaussian flanks, that define the area of evaporation. In fact we can measure this distance under an optical microscope, when we investigate evaporated regions of our source window (3.5).

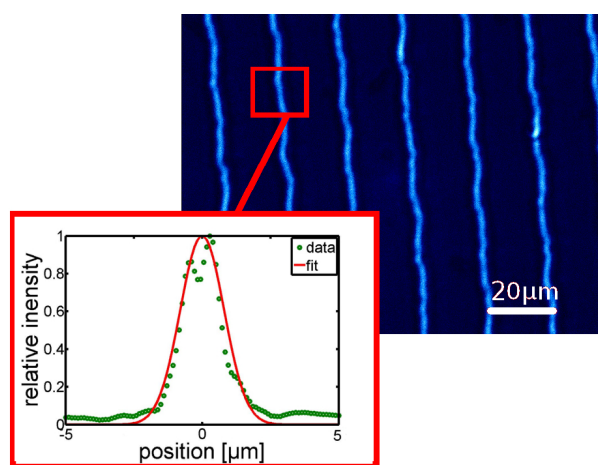


**Figure 3.5** Picture of few layers of phthalocyanine molecules after laser evaporation in our source. Remaining molecules are still dark blue whereas evaporated areas are brighter. The fitting of these stripes with a Gaussian profile results in a full width with half maximum of about 1.6  $\mu\text{m}$ .

To be able to control the laser spot size in situ we image the fluorescence of the molecules during the evaporation process onto a CMOS camera. The dark stripes in picture 3.6 correspond to evaporated parts of the sample, while the bright areas represent fluorescing molecules in situ.

The elongated shape of our evaporation area is reflected in the coherence of the molecular beam. In our setup we scan in the vertical direction so that a higher precision of our velocity selection can be reached. Nevertheless we cannot measure the source size in the scanning direction so that our calculations handle with



**Figure 3.6** Picture of the fluorescing molecules excited with the source laser during the evaporation process.

1.6  $\mu\text{m}$ , which corresponds to the full width at half maximum of a Gaussian profile that fits to a microscopic picture of our source window after evaporation like it is shown in figure 3.5.

- *Coating technique:* Experiments have shown that phthalocyanine molecules are very stable and give good results when they are heated by a 405 nm laser beam with about  $10 \text{ W}/\text{cm}^2$  power. Quite different to that the family of rhodamine seem to be destroyed by that technique so it has to be carefully heated in an oven. With the described techniques just a few hundred layers of molecules can be placed on the inside of our vacuum window.

One can also drop a solution of molecules onto the vacuum window such that a layer of up to  $50 \mu\text{m}$  thickness is left. That usually results in a very intense signal because the laser spot evaporates a larger amount of molecules each time. The source objective that focuses the laser has got a numerical aperture of 0.55, which would result in an increased source spot size of about  $33 \mu\text{m}$ . Molecules coming from a different spot within a broadened source will build up a slightly shifted interferogram resulting in broadened interference peaks. However, in the experiment the impact is orders of magnitude smaller than theoretically expected. Therefore we assume that the small steps ( $\leq 10 \mu\text{m}$ ) of the vacuum stage, which moves the source window partly, compensates this effect.

Taking formula (2.6) from theory and molecules with a mean *de Broglie* wavelength of  $\lambda_{dB} = 5 \text{ pm}$  we reach a spatial coherence of about  $4.7 \mu\text{m}$  at the position of the

grating. This means, that with a grating of 100 nm periodicity we can illuminate about 47 slits of the grating in a coherent way with our matter waves.

For practical reasons the amount of collected signal at the detection plate is counted in values of evaporated loops. Due to the fact that we can not work with an infinitely long vacuum window, we have to scan with the laser in several stripes (see figure 3.7). One loop is then associated to the area the source laser evaporates during the stage with the vacuum window is moved up and down once. Usually we evaporate stripes of 3 mm length, which means that one loop corresponds to about  $4800 \mu\text{m}^2$  of coated area lifted. Due to the strict collimation, on average just one molecule reaches the detector per second.

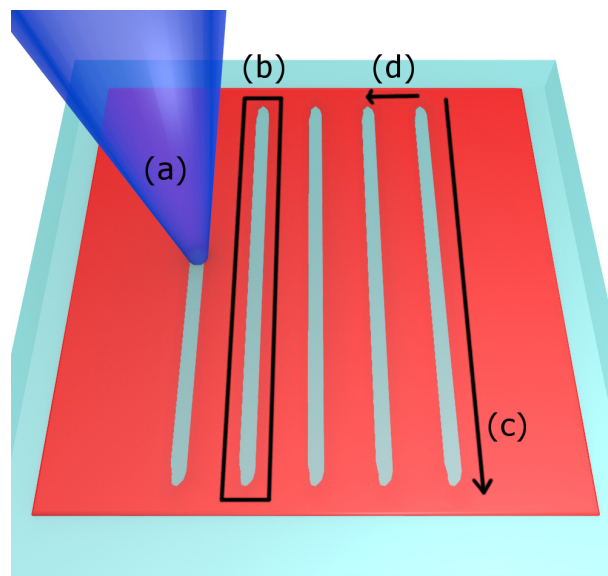


**Figure 3.7** Sketch of the source scanning process. a) scanning laser, b) area of one loop, c) scanning direction, d) scanning steps.

### 3.3 Beam preparation

- *Source size control:* This component is realized by a slit of  $1 \mu\text{m}$  width written in a  $\text{SiN}_x$  membrane. It is placed  $874 \pm 3 \text{ mm}$  after the source and has the task to reduce the beam width. It can be treated like a new source position with fixed dimensions. That is useful if one is not sure about the stability of the source conditions such as the thickness of the molecular layer on the source window or

the size of the evaporation spot. Under normal conditions where the source size at the coated window is about 1.6  $\mu\text{m}$  the slit is not necessary, because the coherence of the source is sufficient.

- *Horizontal collimation, S1X and S2X:* Those two elements are slits with a piezoelectric control in the horizontal axis orthogonal to the molecular beam. It is possible to limit the beam size in this direction from about 210  $\mu\text{m}$  down to 5  $\mu\text{m}$  in a controlled way. Whereas *S1X* is mounted about a meter downstream from the source, *S2X* is just a few mm in front of the grating. That allows us to block imperfections or defects in the membrane and to establish the required collimation angle  $\theta_{coll} \leq 10 \mu\text{rad}$ . Those two slits are fixed in their position, so that one can use them as a reference, to which the whole setup is always aligned.
- *Vertical collimation, S1Y and S2Y:* These slits provide vertical control over the beam. They are fixed in their width, but we can select from a number of slits at the same position. Only *S1Y* was mounted when the rotatable grating holder was in place. Most of the time we use a 5  $\mu\text{m}$  slit at *S1Y* to obtain a good velocity selection of our molecular beam. This mechanism will be described in more detail in the following section.

### 3.3.1 Velocity selection

At the source we start with an evaporation process that produces a *Maxwell-Boltzmann* like distribution of velocities. After about one meter we place the first velocity selection slit, *S1Y*, into the beam  $466 \pm 3$  mm in front of the grating. Every molecule with a different velocity has got its own flight parabola in the gravitational field defined by the source, *S1Y* and the height on the detector. At a certain height of the detector plate we will thus collect a certain class of velocities. The velocity selection slit cannot be infinitely small. The width of the velocity distribution at the detector will be wider for faster velocities. With a 5  $\mu\text{m}$  slit at *S1Y* one can define the mean velocity at a certain height. For a velocity of 200 m/s a precision of  $\frac{\Delta v}{v} \approx 10\%$  can be reached.

Note that the *Maxwell-Boltzmann* distribution might look a bit different on the detection plate because each velocity undergoes a bullet free flight, starting at the source. Depending on the most likely velocity in the distribution, the intensity of

velocities on the detector will reflect the source settings. Therefore, a velocity spectrum of phthalocyanine molecules will look different to a spectrum of rhodamine in the end (see figure 3.8 for the comparison of those).

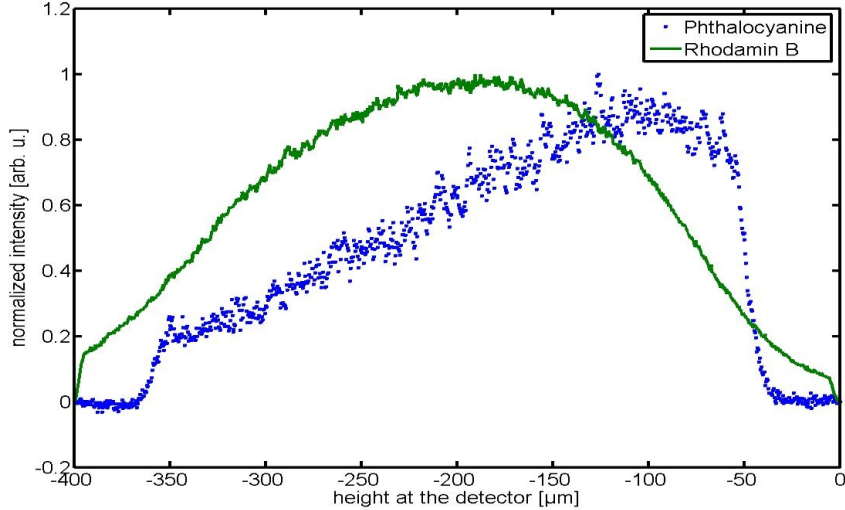


**Figure 3.8** Intensity of the signal depending on the height on the detector (experimental data). This should reflect the *Maxwell-Boltzmann* distribution combined with the bullet free flight through our velocity selection slit. From the most probable velocity of the distribution  $v_{max} = \sqrt{\frac{2k_B T}{m}}$  one can follow the temperature of the source to be about 2000 K for phthalocyanine, whereas it is just 1500 K for rhodamin B. This discrepancy reflects the different evaporation temperatures of the molecules.

With the knowledge of that it is possible to model the distribution one expects at the detector. From the diffraction condition we also know the velocity for a certain height. Therefore, we are able to match the experiment with the theoretical model. A detailed description of that can be found in [51].

### 3.4 Diffracting element

Our setup for grating diffraction is very similar to the double slit experiment. Instead of using photons or electrons we use molecules. The *de Broglie* wavelength (2.2) sets an upper limit to the periodicity of the diffracting element. If the coherence conditions are met, we are left with very few molecules at the position of the grating. Thus, it is reasonable to use a grating with many slits instead of just a double slit in order

to collect as many diffracted molecules as possible. Assuming nearly plane molecular waves with a few picometer wavelength we have to choose the grating periodicity to be sufficiently small, so that we can resolve the interference pattern in the end. The lower limit is set by the width of the slits which has to be big enough to transmit the molecules even after taking interaction forces into account.

The goal is a diffracting element with a periodicity of  $d \leq 100$  nm that acts on the wave in a coherent way. This can happen in a way that parts of the molecular beam are blocked resulting in a change of the particles momentum. This is done by grating rods but can also be achieved in other ways, such as ionization [57]. A change of momentum is an essential part of all gratings due to the grating-kick of  $2\hbar k$ . In principle, light as well as material gratings can be used and have already been realized for diffraction[12,72].

In the current setup we use material gratings made of a thin membrane of silicon nitride or carbon. In this membrane the gratings are milled with a focused gallium ion beam by the group of Prof. Ori Chesnovsky at the University of Tel Aviv. This enables us to use gratings with 100 nm periodicity and a thicknesses between 95 nm and a few nm. Current studies are even investigating gratings milled into single layer graphene sheets. Those are expected to limit the *van der Waals* interactions between the grating and the molecules to a minimum. The fabrication of such gratings is at the limit of current nanotechnology. Not only the periodicity and the thickness define our interference pattern, but also the opening fraction. It is possible to make 5 nm thick  $SiN_x$  gratings with an opening fraction up to about 80%.

grating \ property	thickness	opening fraction	periodicity	material
<b>G1</b>	10 nm	0.46	100 nm	$SiN_x$
<b>G2</b>	46 nm	0.46	100 nm	$SiN_x$
<b>G3</b>	10 nm	0.75	100 nm	$SiN_x$
<b>G4</b>	87 nm	0.57	100 nm	$SiN_x$
<b>G5</b>	21 nm	0.68	100 nm	<i>Carbon</i>

**Table 3.1** List of the gratings used in the matter wave interferometric setup and their properties measured with a transmission electron microscope.

Due to the production process with a focused gallium ion beam, the walls of the grating slits have a certain wedge-angle with respect to the centerline (see figure 2.5). This angle is about 10 degrees for thick gratings and gets bigger as the thickness decreases.

For an investigation of effects rising from the rotation of a grating with respect to the molecular beam, as they are described in the theoretical part of this work, a special mount for our gratings was designed and built. The plans and visualizations of that can be found in the appendix (7.1). With this grating holder it is possible to rotate a grating up to 82 degrees. However, the finite membrane thickness limits the rotation so far to 60 degree, for a 5 nm thin  $SiN_x$  grating.

For the studies on polar particles grating *G5* was chosen from table 3.1. This grating is milled into a amorphous carbon membrane, that is supported by a copper mesh (see figure 3.9). The large opening fraction and the low thickness guarantee a good transmission of the molecular signal. Another advantage is the possibility to rotate the grating up to about 50 degree, because of the thin supporting copper structure. All the other gratings are supported by a 100 to 200  $\mu\text{m}$  thick  $SiN_x$  frame that limits the rotation to less than *G5*.

### 3.5 Detection

The detection is defined by a thin quartz plate that collects the molecules. Once the molecules stick on the detection plate, we are able to observe them using a fluorescence microscope. The signal is collected by a camera with a  $1003 \times 1004$  pixel CCD chip. Each pixel has a size of 8  $\mu\text{m}$  so that using a 20x or 40x objective results in 200  $\mu\text{m}$  or 400  $\mu\text{m}$  wide field of view, respectively. The quartz plate is illuminated from the backside with a rectangular shaped laser spot coming from cw diode lasers centered at wavelengths of 661 nm or 532 nm. The square is produced by retro reflection of the laser beam from the binary mask of a spatial light modulator.

After the objective a suitable fluorescence light filter transmits the fluorescence of the collected molecules and blocks the exciting laser light. With this technique we are able to observe each single molecule that sticks on the quartz plate. The optical resolution in a microscope is given by the *Abbe*-limit [58] so the minimal feature size we can resolve is about 300 nm for rhodamin molecules.

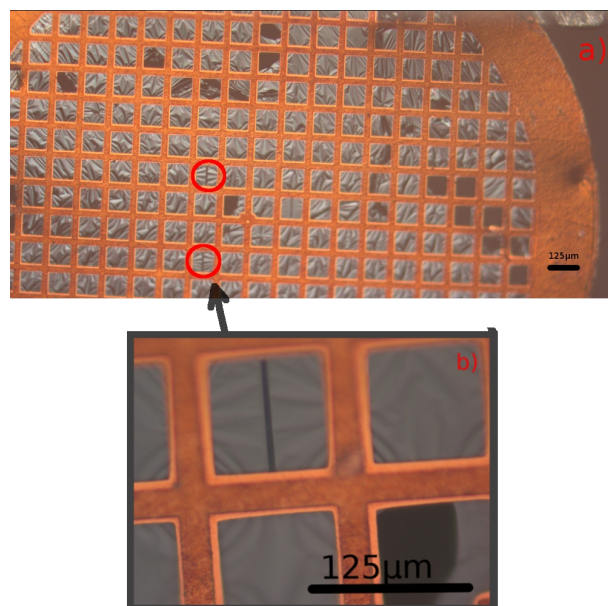


**Figure 3.9** Overview (a) and detailed view (b) of the carbon membrane supported by the copper mesh. The gratings in (a) are written in the area indicated by the red circles. Defects in the carbon membrane such as holes next to the grating sometimes help during the alignment because they usually transmit much more signal than the grating itself. In (b) the support structure of the grating can be seen.

This is bigger than the size of a single molecule, but by collecting enough photons from each fluorescing molecule it is possible to fit the center of the point-spread function to localize each single molecule with about 10 nm accuracy [59,60].

This is based on the assumption that the molecules stick on the surface of the detection plate. However, surface diffusion could affect the interference contrast even within the time span of the interference collection. For phthalocyanine molecules this is very unlikely to happen. Studies of an interference pattern over about 72 hours did not show any movement of molecules over time as can be seen in figure 3.10. Further studies included the collection of signal coming from molecules directly after their arrival. While the signal was collected pictures with an accumulation time between two seconds and two minutes were taken. In this case it was possible to assign the signal to single fluorescing molecules which means that they did not travel far enough to wash out the interference pattern. Typical surface diffusion rates referred in literature [61,62,63] lie in the range of  $\mu\text{m}^2/\text{s}$  and would have been observable in these kind of studies.

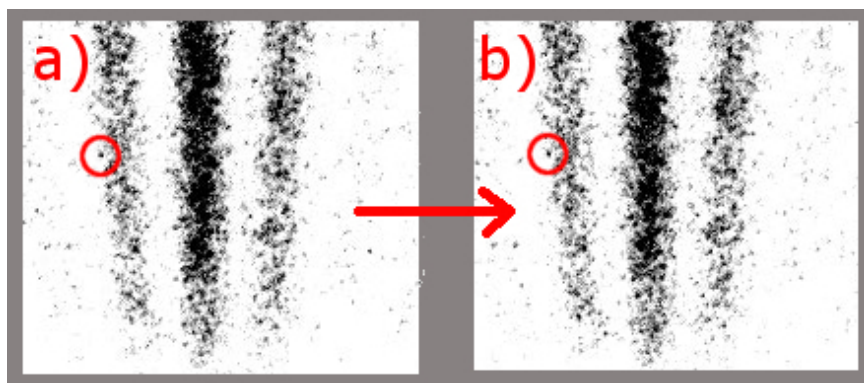


**Figure 3.10** Investigation of a phthalocyanine interference pattern (a) before and (b) after a period of 72 hours. We see that the position of single molecules does not change over time.

For rhodamin molecules not all of those studies were performed. Furthermore, some references [64] leave doubts about the immobilization of rhodamin molecules at surfaces so that we can not fully exclude it yet.

### 3.6 Molecules

It is essential that the molecules fluoresce in order to see them in this setup. The current experimental setup includes detection lasers of a wavelength at 532 nm or 661 nm respectively. Thus, sufficient absorption in this region for the molecule of interest is important. In principle, other detection wavelengths can be implemented into the setup as well. The fluorescence afterwards is distinguished from the excitation by a certain filter, that is in accordance with the spectrum of the molecule. Further, it is necessary that the molecules are thermally stable in order to ensure to lift them into the gas phase intact. Molecules in a diffraction setup as described in this work, are theoretically suited up to a mass of about 10.000 atomic mass units. In the current setup the molecular mass that can be handled is mainly limited by the periodicity of the gratings we use. For a good differentiation of the interference peaks they have to be at least 10  $\mu\text{m}$  apart from each other. Taking molecules traveling at a speed of 150 m/s through a grating of 100 nm period sets the upper mass limit to about 1500 atomic mass units. The following three molecules were chosen because they were expected to fulfill the requirements of the diffraction experiment in a good way.

### 3.6.1 Phthalocyanine

Phthalocyanine has the chemical formula  $C_{32}H_{18}N_8$  and its structure is shown in figure 3.11.

It is well suited because it is very stable even when it is heated to temperatures up to 2000 K. It is also interesting as it may be modified chemically. Chains of different atoms may be attached leading to more massive particles with similar stability and fluorescence properties. It has got a molar mass of 514,54 g/mol. In our setup this leads to *de Broglie* wavelengths of about 3 to 5 pm for molecular velocities of 150m/s to 400m/s respectively. It has been reported to have a quantum yield of 0.6 [65] and an absorption- and fluorescence-spectrum that fits well to the experimental approach of single molecule detection(see 3.12 and 3.13).

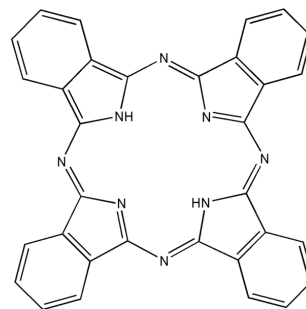


**Figure 3.11** Schematic drawing of the phthalocyanine molecule.

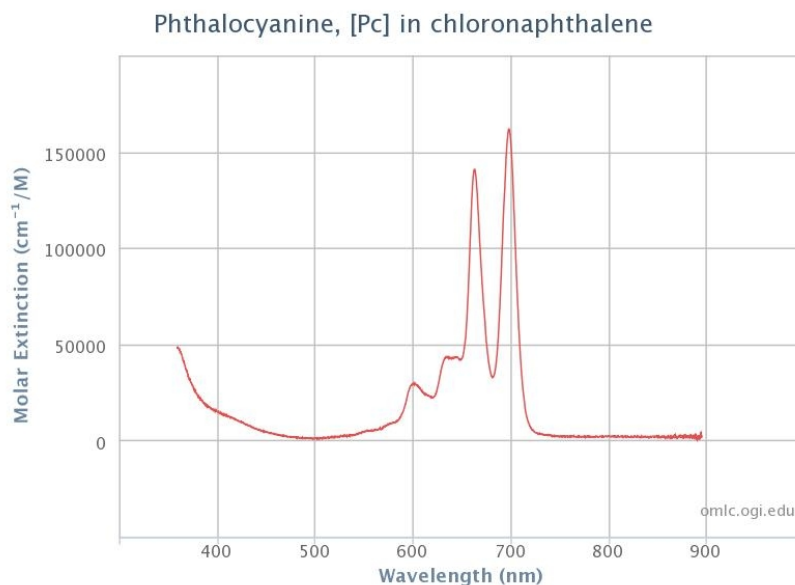


**Figure 3.12** Absorption spectrum of phthalocyanine in chloronaphthalene in scales of the absorbance per molar concentration and centimeter [i].

We use the absorption peak at 664 nm to excite the molecule with a laser of 661 nm wavelength. With a Bright Line fluorescent filter 711/25 we then select the light emitted by the molecules on the detection screen.

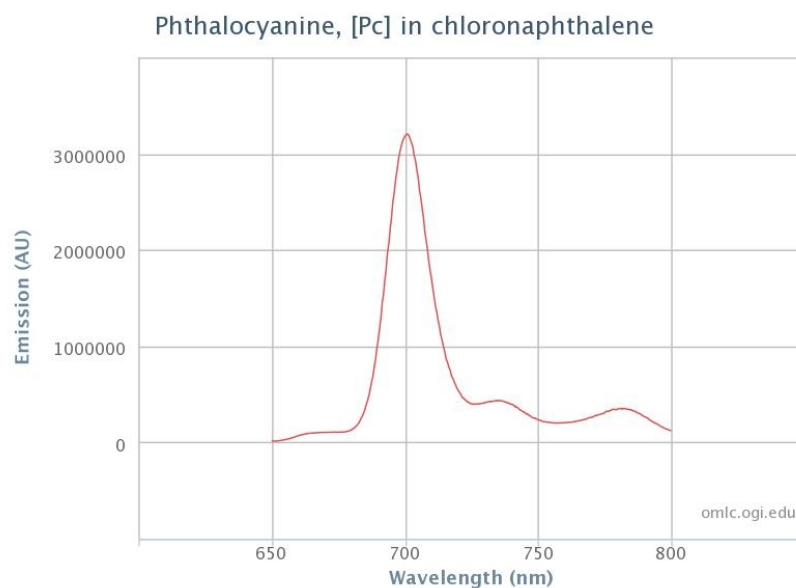


**Figure 3.13** Fluorescence spectrum of phthalocyanine in chlornaphthalen excited at 635 nm [ii].

### 3.6.2 Rhodamine 6G

Contrary to phthalocyanine rhodamine 6G has a permanent dipole moment, which amounts to about  $6\text{ Debye}$  due to the chlorine atom. Its chemical formula is  $C_{28}H_{31}N_2O_3Cl$ . It has a mass of  $479.02\text{ g/mol}$  and provides a fluorescence quantum yield of  $0.9$  [66].

There is some evidence that some of the rhodamine molecules decompose above a certain temperature (see figure 4.8). However, experiments [67] indicate that a thermal evaporated beam of rhodamine molecules stays stable in the gas phase. Comparing the interference pattern of selected velocities with the one of phthalocyanine additionally allows us to calculate the mass of the interfered molecules, which mainly seems to be the one of the intact molecule. Still from the interference pattern (as we will see in section 4.1) some doubts remain if all of the molecules stay intact during the evaporation process.

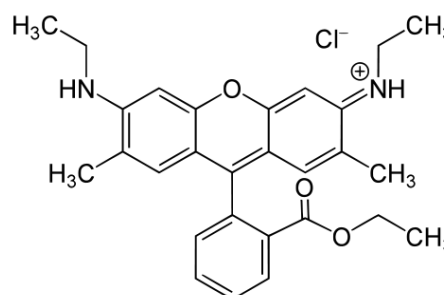


**Figure 3.14** Schematic drawing of the molecule rhodamine 6G.

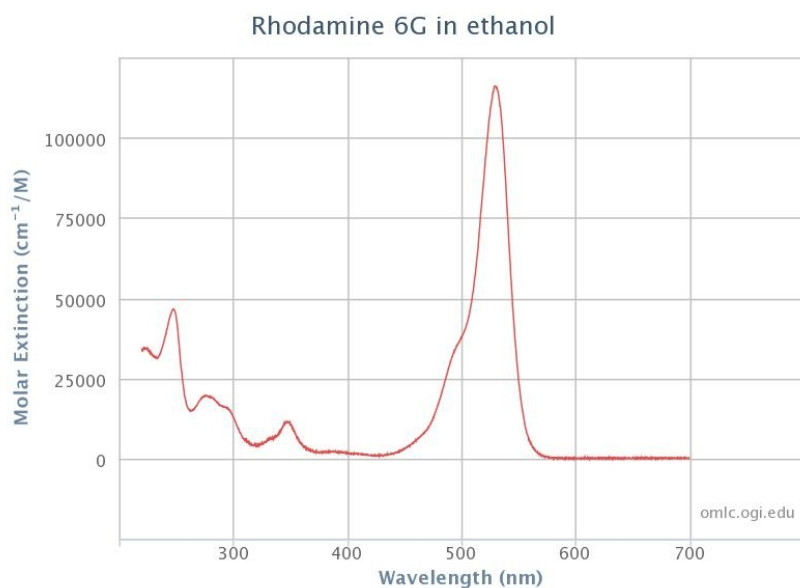


**Figure 3.15** Absorption spectrum of rhodamine 6G in ethanol in scales of the absorbance per molar concentration and centimeter [iii].

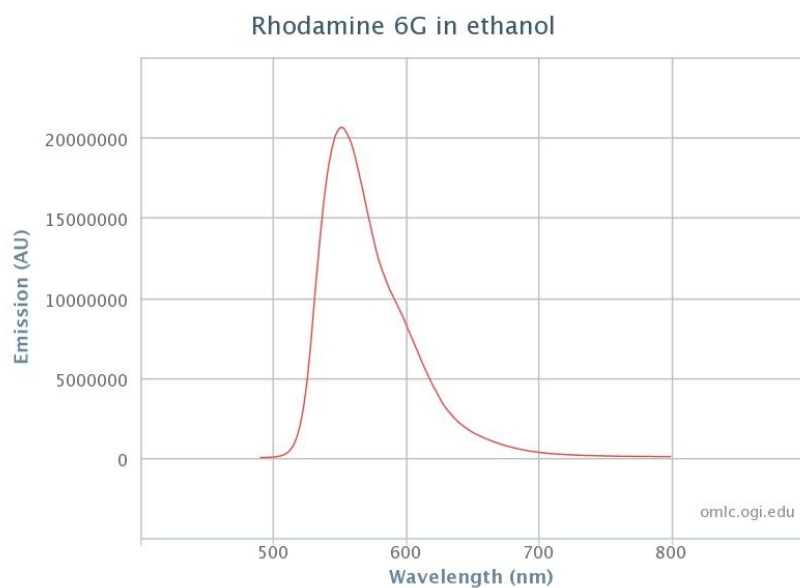


**Figure 3.16** Fluorescence spectrum of rhodamine 6G in ethanol excited at 480 nm [iv].

At the detector we excite rhodamin 6G with a wavelength of 532 nm, which is very close to the absorbance maximum and filter its fluorescence light with a Carl Zeiss BP 550/25 fluorescence filter.

### 3.6.3 Rhodamine B

According to density functional theory [68] rhodamin B has a dipole moment of about 9.8 *Debye*. It has the same mass as rhodamine 6G and its chemical formula is  $C_{28}H_{31}ClN_2O_3$ .

A quadrupole mass spectrum of this molecule taken with our source setup is shown in section (4.1). It indicates that the rhodamine molecules break into several different fragments. Each of these has different properties like the permanent dipole moment and polarizabilities. However, a clear differentiation between the fragmentation at the source and the ionization in front of

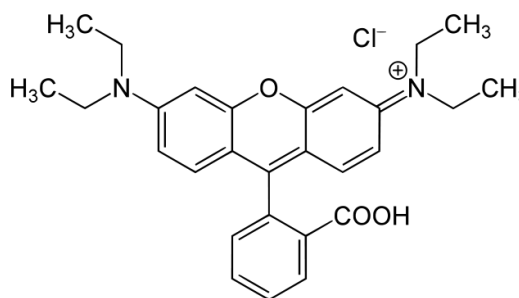


**Figure 3.17** Schematic drawing of the molecule rhodamine B.

the quadrupole is not possible. As we will see in chapter 4 it is not possible to fully explain the experimental data with those fragments. Rhodamine B is similar to rhodamine 6G in its absorbance and fluorescence properties (compare 3.15 and 3.16 with 3.18 and 3.19), so that we can detect it with the same detection setting as we use it for rhodamin 6G.

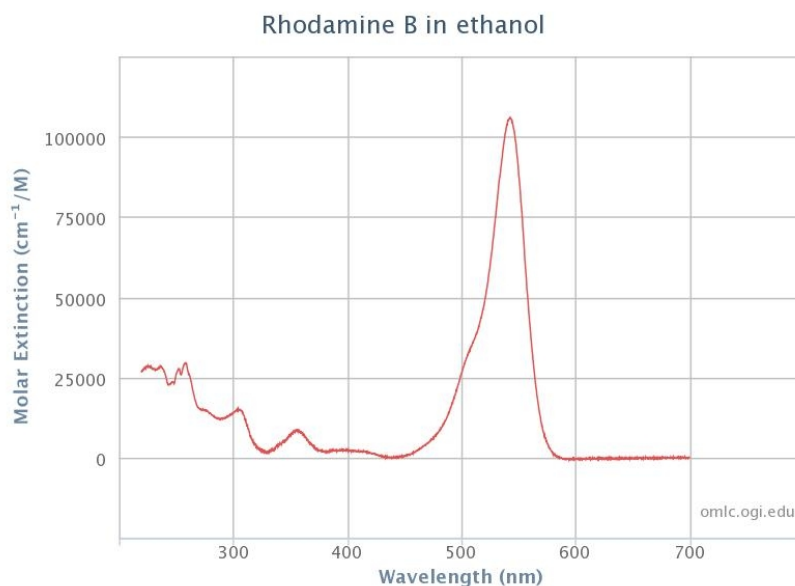


**Figure 3.18** Adsorbition spectrum of rhodamine B in ethanol in scales of the absorbance per molar concentration and centimeter [v].

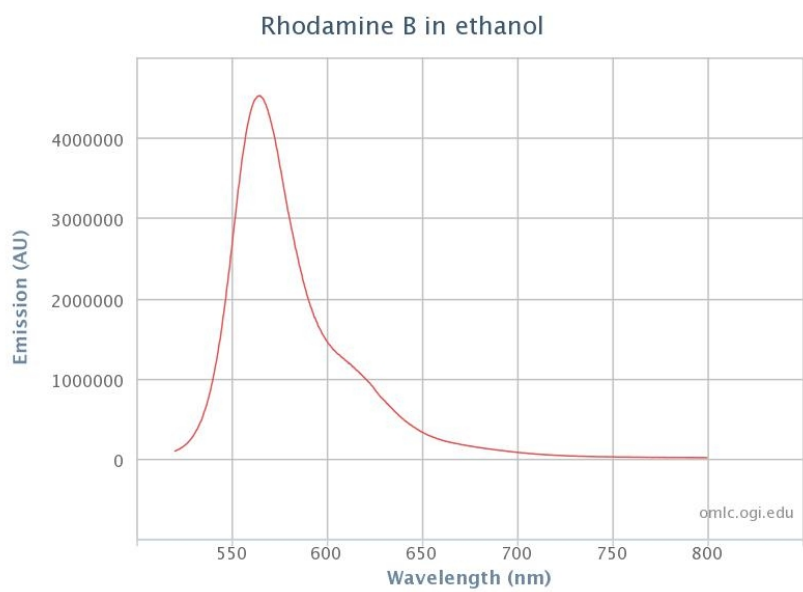


**Figure 3.19** Fluorescence spectrum of rhodamine B in ethanol excited at 510 nm [vi].

# 4 Experimental data

## 4.1 Polar particles

The complexity of molecules make them distinguishable by several different properties. One of these is the separation of charges in certain parts of the molecule leading to a permanent electric dipole moment. A lot of biomolecules exhibit such a polar structure. It is therefore interesting to investigate such particles and to learn about their behavior in interferometry experiments. The interaction between a dipole close to a wall and its induced mirror dipole should be stronger than the *van der Waals* forces between molecules.

In order to investigate polar particles systematically we chose the three molecules already mentioned in section 3.6, which exhibit dipole moments of about zero, six and ten debye. This should enable a first step into the investigation of a scaling behavior in the molecule-grating interaction. Further, we decided to combine this with the option to rotate the grating with respect to the molecular beam. The effect on the molecular beam is twofold as described in section 2.3.3. It reduces the effective opening fraction as well as the grating periodicity in the direction of the molecular beam. The effect of the smaller opening fraction should directly influence the population of the interference orders due to the fact that a larger percentage of molecules are affected by a steeper part of the grating potential.

## Measurements

In a first step a series of data was taken for rhodamine B and rhodamine 6G. Laser evaporation-coating was not possible for these molecular species. The reason was not verified but we attribute it to decomposition of the molecules due to excessive heating. Due to those technical issues in the coating technique first studies were carried out with a 'droplet' source. One interference pattern collected this way is shown in figure 4.2. The investigation of the source spot size under a microscope (figure 4.1) was done like for phthalocyanine in figure 3.5. This data shows a source spot size of about 5.5  $\mu\text{m}$ . Compared to the spot size of 1.6  $\mu\text{m}$  that can be reached on evaporation coated phthalocyanine layers, the broader source spot reduces the molecules transverse

coherence. Taking a molecular wavelength of  $\lambda_{dB} \approx 5$  pm for equation (2.6) the width of the coherently illuminated area reduces from about 4.7  $\mu\text{m}$  to about 1.4  $\mu\text{m}$ . It means that instead of 47 there would just be about 14 slits illuminated in a coherent way. From the first interference pictures (left picture of figure 4.2) this assumption seemed to be reasonable.

To reach the same level of coherence for rhodamine molecules as for phthalocyanine, we changed the source window preparation. We filled an oven with molecules and placed it in a small distance in front of the vacuum exposed side of the source window glass. As the oven is heated up to about 540° K the molecules evaporate and stick on the colder glass to cover it with a few layers of molecules. With this technique it was possible to compare the rhodamine molecules with the phthalocyanines under the same source size conditions. The right picture of figure 4.2, using the vapor deposited source window is qualitatively still not comparable to those of phthalocyanine (e.g. 4.3). This indicates that other effects do play a role in the smearing of the interference.

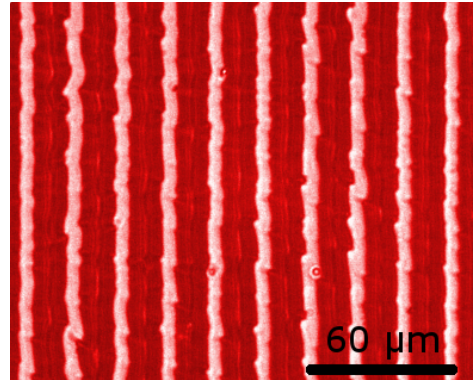


**Figure 4.1** Picture of a source window coated with rhodamine 6G molecules with the dropping technique. Bright stripes are where the laser evaporated the molecules.

To better understand the role of the molecule-grating interaction a second set of data was taken for grating rotation angles of 0, 10, 20 and 30 degree with regard to the molecular beam. An overview over this data is shown in figures 4.3 to 4.5. For these plots a representative velocity of 260 m/s was selected in the raw data (as e.g. 4.2), corresponding to a certain height at the detector. This velocity is the same along a horizontal line in the interference data, around which a stripe of fifty pixels is usually vertically integrated to obtain a better signal-to-noise ratio.

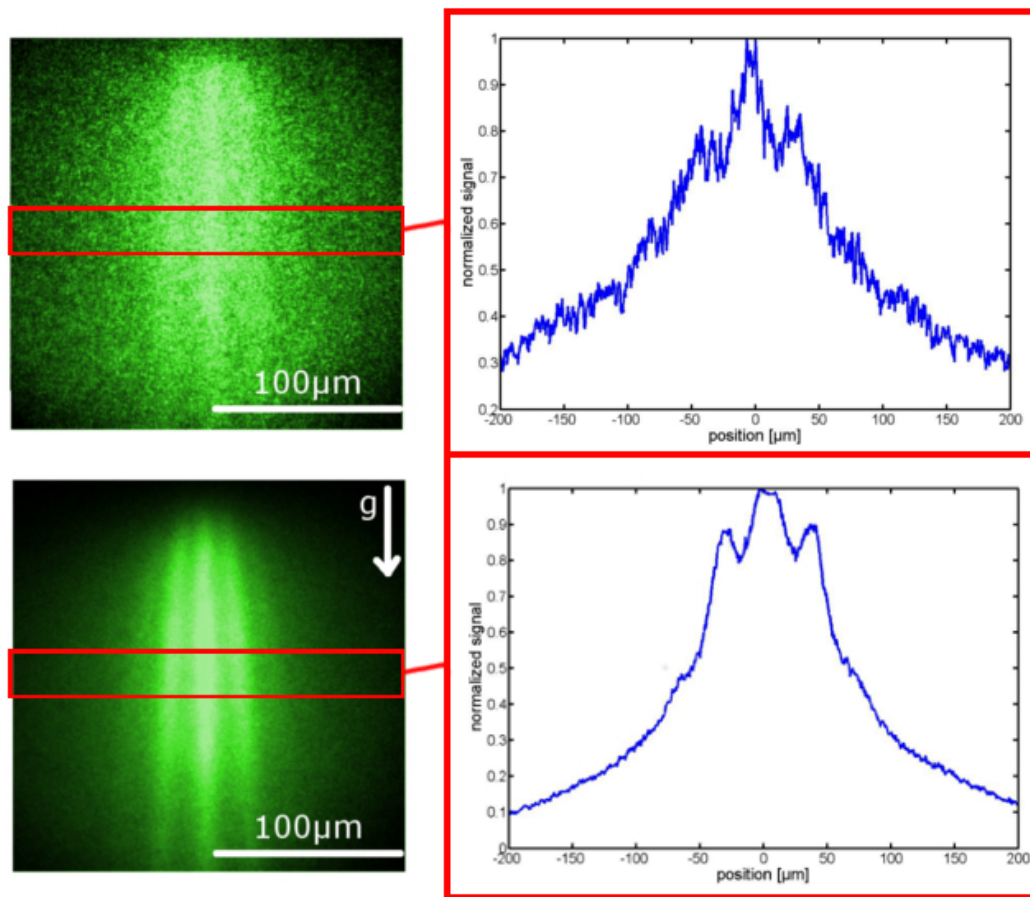


**Figure 4.2** Comparison of interference pictures of rhodamine B, collected with a droplet coated source window (upper pictures) and an evaporation coated source window (oven approach) (lower pictures). The background is lower in the second case. The quality of the interferogram is still not comparable to those of phthalocyanine (e.g. figure 4.3).

## Results

A lot of effort has been made to keep the experimental settings the same for all molecules. Still the quality as well as the signal intensity of the interference fringes for polar particles varied a lot. A systematic behavior in all our dipole studies is shown in figure 4.6. When the grating is rotated one would expect a smaller effective slit width of the grating and therefore a stronger population of higher order interference fringes. This matches with theory for all molecules. Similarly, one would expect a smaller effective slit width for bigger dipole moments of the molecule. To check this relation the experimental data was evaluated by fitting the single peaks of the interferogram with a parabola. The intensities of the first diffraction orders were compared to the zeroth order. Each molecular species was investigated with the same grating.

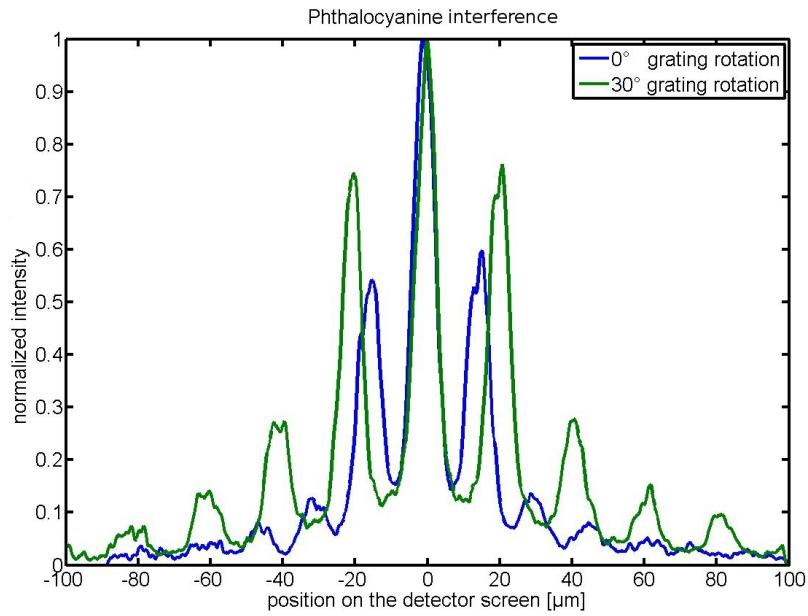


**Figure 4.3** Intensity profile at the detector for phthalocyanine molecules for  $0^\circ$  and  $30^\circ$ . The data corresponds to a mean velocity of  $v \approx 260\text{m/s}$  with  $\Delta v/v \approx 10\%$ . For the rotated grating the peak separation increases due to the smaller slit opening (see equation 2.26) and higher diffraction orders are more populated.

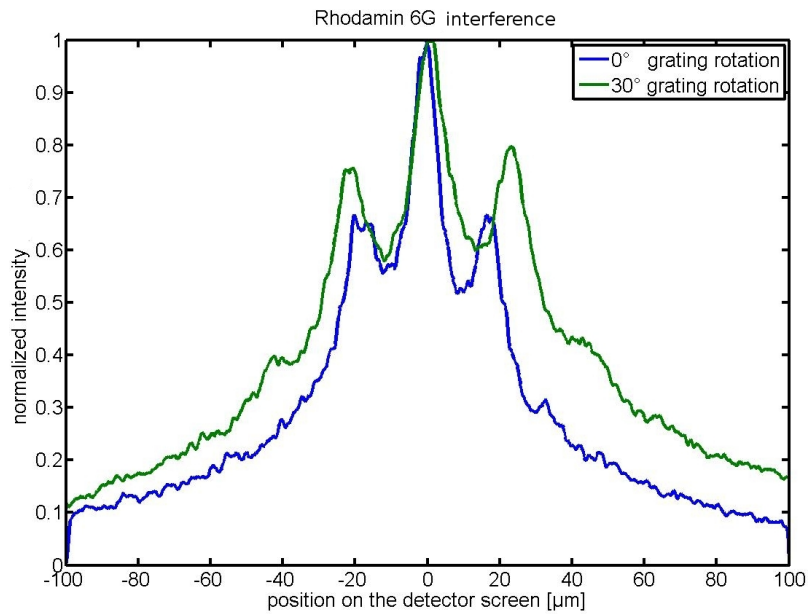


**Figure 4.4** Intensity profile at the detector for Rhodamin 6G molecules for  $0^\circ$  and  $30^\circ$ . The data corresponds to a mean velocity of  $v \approx 260\text{m/s}$  with  $\Delta v/v \approx 10\%$ . From the first diffraction order we follow that the peak separation increases with the rotation angle of the grating. Due to a growing background higher diffraction orders may just be assumed.

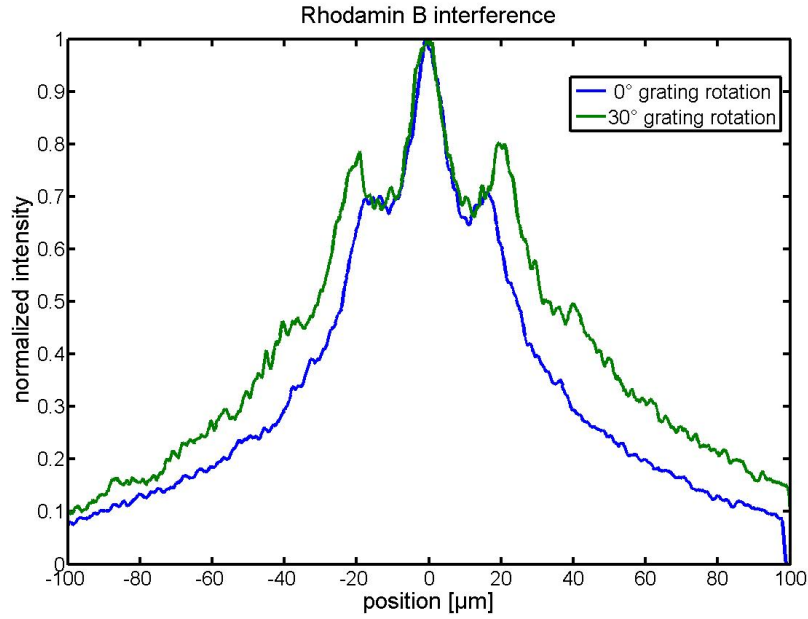


**Figure 4.5** Intensity profile at the detector for Rhodamin B molecules for  $0^\circ$  and  $30^\circ$ . The data corresponds to a mean velocity of  $v \approx 260\text{m/s}$  with  $\Delta v/v \approx 10\%$ . From the first diffraction order we follow that the peak separation increases with the rotation angle of the grating. Due to a growing background higher diffraction orders may just be assumed.

Thus, small imperfections in the grating that would lead to a higher population of the zeroth diffraction order cancel out in the comparison. Since the statistical error from the fit was rather small (below 5%) figure 4.6 shows the data points for the positive (cross) and the negative (ring) first order separately. These points were then compared with a model based on the fitting routine described in [53] and [51]. It makes use of the *Fraunhofer* approximation (2.11) described in section 2.2 and produces an interferogram for each velocity of interest. From theory one would expect that an increase in molecular dipole moment leads to an increase of the interaction potential (see 2.24) and a stronger population of higher order interference peaks. An evaluation of the measured data relies on the fact that the investigated molecule as well as its dipole moment stay intact. Later studies at a quadrupole mass spectrometer (see figure 4.8) suggest that fragments contribute to our interference pattern. However, a difference between molecules with different dipole moments is evident in the data and may tentatively be correlated to a stronger interaction.

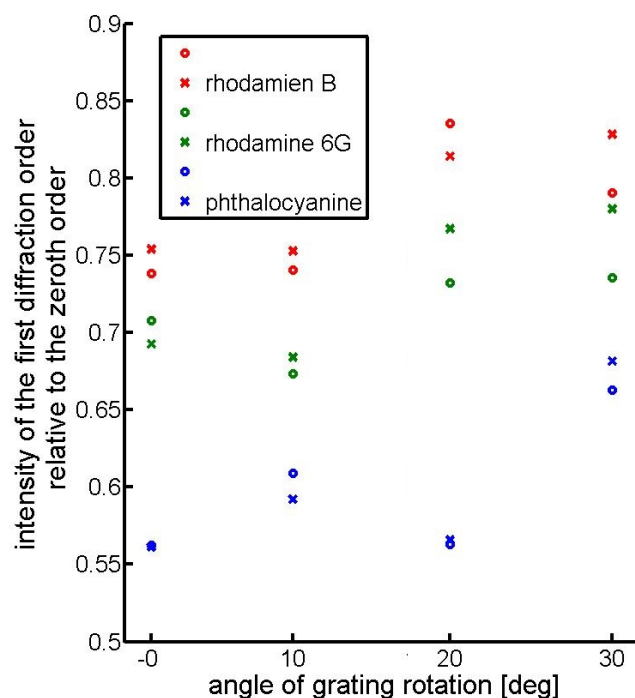


**Figure 4.6** Intensities of the first interference order relative to the zeroth order diffraction intensity under the rotation of the diffraction grating. As the angle of grating rotation increases, the relative amplitude of the first interference order does. An increasing dipole moment of the molecule seems to increase this magnitude as well. Due to a relatively small statistical error of the fit the data points for the first order (ring) and the minus first order (cross) relative to the zeroth order of diffraction is shown.

Already an evaluation by eye shows that the quality of the interferogram for rhodamin differs from the one of phthalocyanine. Some effects that might cause this are discussed in the following:

- *Laser evaporation source:* Our molecular source works with a laser that heats the molecules to lift them into the gas phase. For rhodamine molecules we had to use different source preparation techniques. To check, whether intact molecules are lifted into the gas phase, the source setup was attached to an *Extrel* quadrupole mass spectrometer (see figure 4.7) that detects molecules ionized by a filament. Results of that measurements are shown in figure 4.8 and indicate that only fragments of rhodamin B reach the detector.

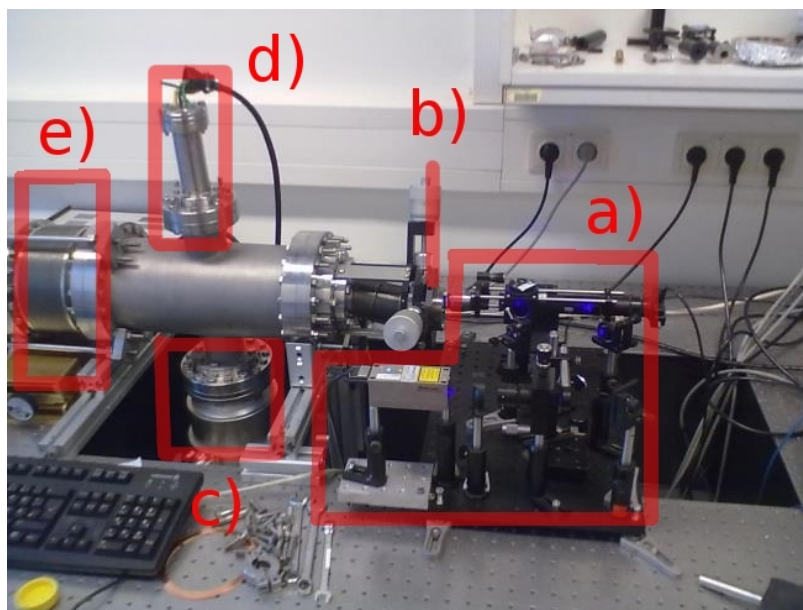


**Figure 4.7** Experimental setup for the quadrupole mass spectrometry of rhodamine B and phthalocyanine. a) laser evaporation source, b) coated source window, c) turbo molecular pump, d) vacuum gauge, e) *Extrel* quadrupole mass spectrometer.

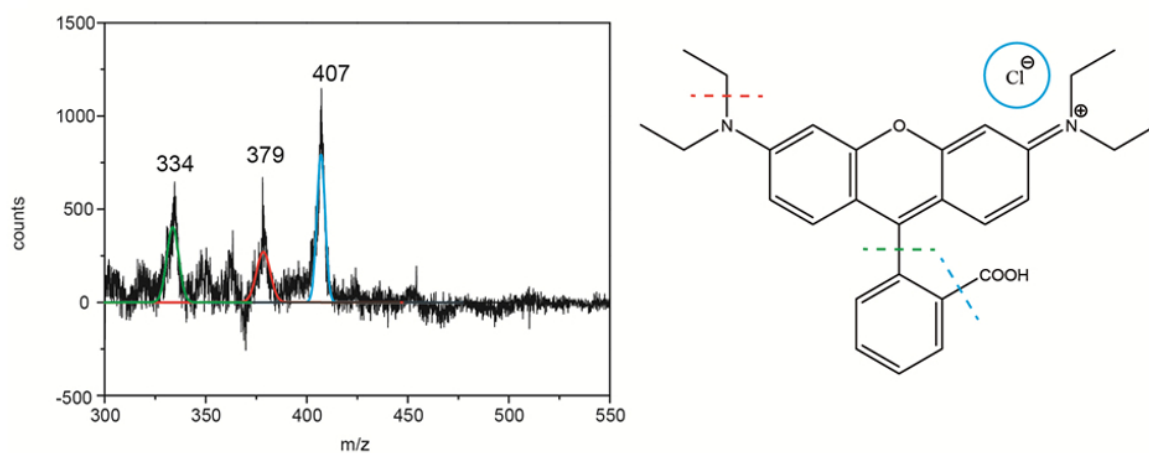


**Figure 4.8** Quadrupole mass spectrum of rhodamin B evaporated with the laser evaporation source of the diffraction setup (left). Compared to literature [69] the peak in blue corresponds to 400 atomic mass units. The red peak corresponds to 371 and the green one to 324 atomic mass units. On the right side possible points of fragmentation in the molecule leading to the measured fragments are shown. Note that the parent mass was not present. [vii]

Yet, the interpretation of the electron impact is not fully clear. The molecule may also break during the ionization process that is needed for the detection with the quadrupole mass spectrometer. A fragmentation of the molecule to smaller pieces as shown in 4.8 would enter an incoherent sum over different interference patterns. Such an incoherent sum of diffraction patterns of different masses is shown in figure 4.9. Although the quadrupole mass spectrum did not show any indication for clusters of rhodamine, those would be crucial to explain such a high intensity between the zeroth and first diffraction order.

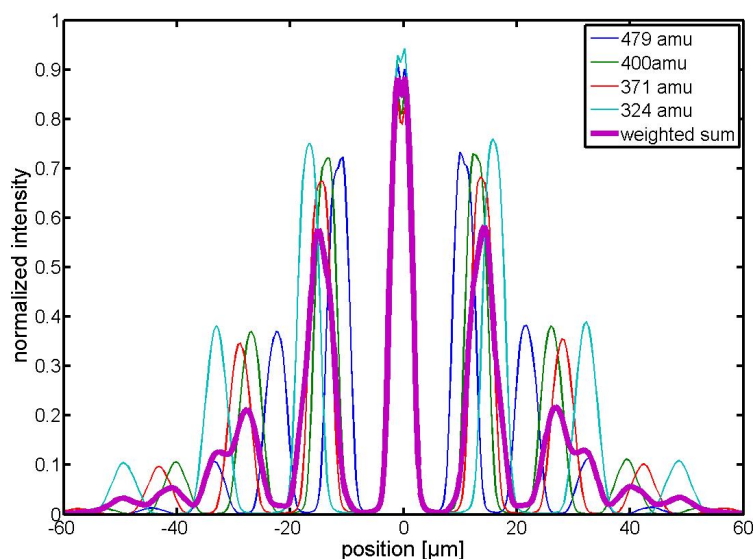


**Figure 4.9** Diffraction patterns of different fragments of rhodamine B and the classical sum of those weighted with their relative intensities as they occur in the quadrupole mass spectrum 4.8.

In this sense a fragmentation of the molecule during the flight can not be excluded but does not explain the experimental results.

- *Molecular rotation:* One degree of freedom is the rotation of the molecule. As already discussed (after equation 2.25) the mean rotational frequencies for rhodamine are in the order of of 80 GHz. For a molecule moving at a velocity of about 250 m/s this corresponds to a distance of about 3 nm in which a full rotation occurs. A material grating, that is much thicker than this distance should average over all different orientations of the molecule. A thinner grating instead interacts quasi-static with different orientations, depending on how the molecules arrive at the grating. In such a case all different interactions sum up at the detector and

may wash out the interference pattern. We can observe, that gratings thinner than ten nanometer do not show any reasonable interference contrast for polar particles.

- *Grating dipole interaction:* Comparing figures 4.4 and 4.5 to 4.3 we see a background growing with the size of the dipole moment. A polar particle undergoes a stronger interaction with a grating wall than a non-polar molecule since the attractive static dipole-dipole interaction adds to the induced dipole-dipole interaction (see 2.25). This might open an additional channel for decoherence effects, such as described for electron beams [55, 56]. There a coherently split electron beam induces mirror charges in a conducting plate, that are dragged by the electron. This dragging causes a current that has to work against the materials resistance leading to dissipation of energy into heat. Due to this effect also the free electron beam undergoes decoherence, manifested in a reduction of the interference contrast. For polar molecules the situation is similar, but instead of a single electron one has two different charges separated by a certain distance.

## 4.2 Discussion of *van der Waals* interactions

This topic is related to former measurements carried out by *Dr. Thomas Juffmann* and *Dr. Michele Sclafani* on this experimental setup [51 and 53]. The aim of these measurements was to show that the influence of the *van der Waals* forces on the interferogram changes with the thickness of material gratings. To shine light on this topic the behavior of phthalocyanine molecules diffracted at different  $SiN_x$  gratings was investigated. The phase that a molecule picks up during its flight through the grating should be directly dependent of the grating thickness described by formula (2.23). This phase is reflected in the interference pattern and thus can be evaluated. A fit was prepared in collaboration with *Prof. Stefan Scheel* and *Dipl.-Phys. Johannes Fiedler* at the University of Rostock. During the evaluation it turned out that the theoretical value of the *van der Waals* interaction constant  $C_3$  differs from the experimental outcome by a factor of ten. Thus, it was necessary to perform further measurements in order to check, whether this discrepancy arises from theory or if it is an error in the measurement.

### 4.2.1 Charges on the grating

Most of the diffraction elements that are used in our setup were fabricated by gallium ion beam milling into thin membranes. These membranes are made of  $SiN_x$ , which is an electrical insulator. From this fabrication process it is expected that charges are left on the grating bars. Due to the impossibility of controlling their position they can destroy the interference contrast or mislead the interpretation of *van der Waals* forces. The theoretical analysis by our collaborators at the University of Rostock showed that our results might be explained assuming the presence of charges on the grating bars. To study their effect, we used a hot tungsten wire to deposit electrons onto the grating. The experimental setup for this sketched in figure 4.10.

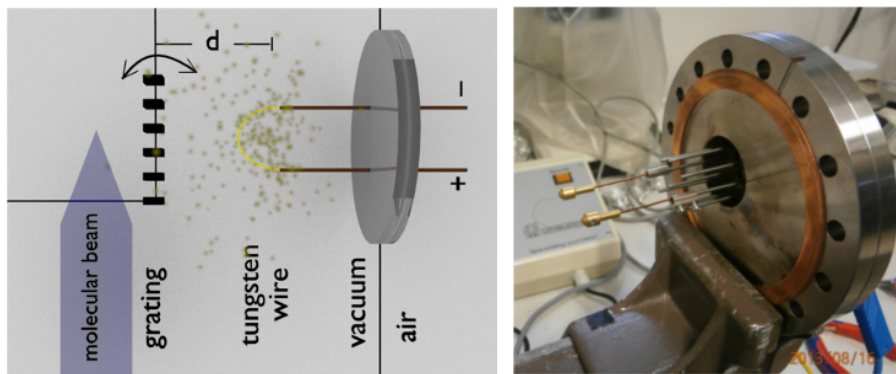


**Figure 4.10** Sketch (a) and part of the realization (b) of the experimental setup to deposit charges on the grating. The grating was mounted on a rotational stage, so that it either could be turned towards the tungsten wire or to face the molecular beam direction respectively.

Our grating was initially mounted on a rotational and translational vacuum stage, so that we were able to place it with its front side in about 6 cm distance to the 0.1 mm thin tungsten wire. Once the wire is connected to a power supply it glows and electrons fly in all directions. Calculating the solid angle that our grating covers at a distance of 6 cm from the wire we can control the number of electrons, that hit the grating by measuring the current through the wire. This is described by the *Richardson-Dushman* equation [70].

$$i(T) = A \cdot T^2 \cdot \exp\left(-\frac{\phi}{k_B \cdot T}\right) \quad (4.1)$$

This formula describes the current per unit area  $i(T)$  resulting from a tungsten wire with  $A = 8 \cdot 10^5 \text{ Am}^2\text{K}^2$  and  $\phi = 4.25 \text{ eV}$  at a temperature  $T$ . To obtain the temperature of the wire this formula is combined with the thermal dependence of the resistance

$$R(t) = R_0 \cdot (1 + \alpha \cdot (T - T_0)). \quad (4.2)$$

For tungsten  $\alpha = 4.5 \cdot 10^{-3}/\text{K}$  [70]. The initial temperature  $T_0$  was assumed to be room temperature at 23 °C.

## Measurements

In a first step the grating was rotated in a way that its front side faced the tungsten wire. Voltage was applied to the wire to achieve a resistance between 7.7  $\Omega$  and 11.1  $\Omega$  for 20 s to deposit the charges on the grating. After that the grating was turned towards the molecular beam and an interference pattern was collected. Step by step, the voltage was increased to deposit more and more electrons on the grating per time. The electron deposition was starting from a few ranging up to more than  $10^7$  electrons, according to formula (4.1).

For phthalocyanine molecules of an average speed of 185 m/s ( $\Delta/v$  10%) and grating G3 figure 4.11 shows representative interference data for all velocity classes.

## Results

Figure 4.11 shows, that the interference patterns lie on top of each other within the borders of normal fluctuation. Electrons on the grating would change the *van der Waals* interaction and thus we would expect a different amplitude for different interference peaks. This is clearly not the case. Measurements performed at the University of Tel Aviv found huge numbers for hole surface densities on  $SiN_x$  membranes treated with focused ion beam methods [54]. According to their studies, hole surface densities of  $10^{10} \text{ Ga}^+/\text{cm}^2$  and higher for ion doses of about  $10^{11} \text{ Ga}^+/\text{cm}^2$  can be imprinted into the surface of the material. During focused ion beam milling of our gratings about

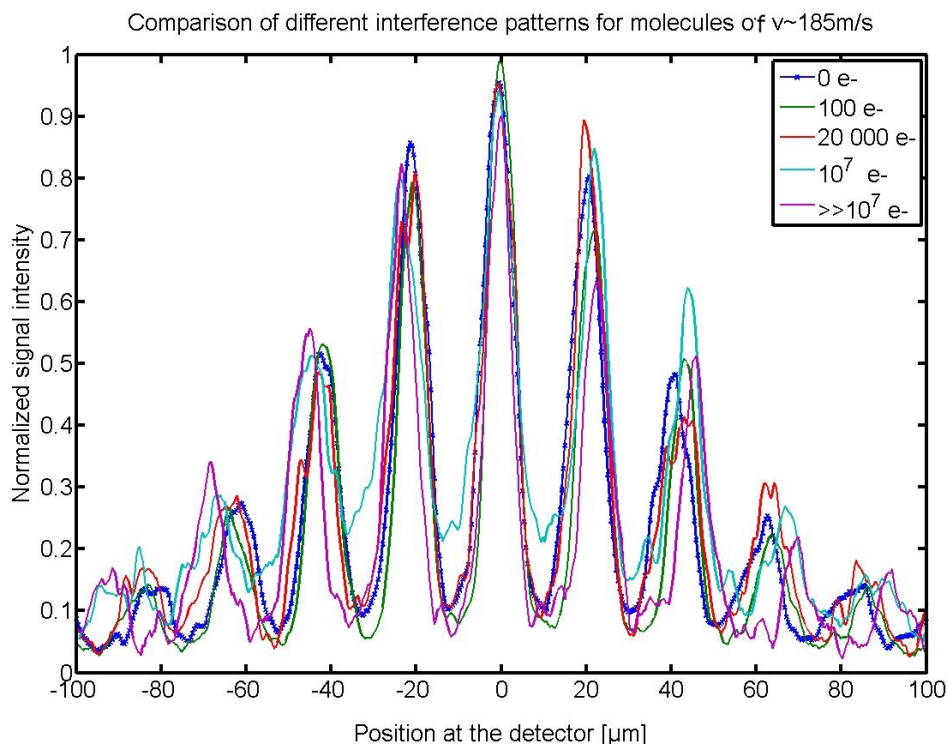


**Figure 4.11** Comparison of interference of phthalocyanine molecules with a velocity of about 185 m/s with the grating 'loaded' with different amount of electrons. Within usual borders of fluctuation the quality of the interference pattern does not change.

$10^7 \text{ Ga}^+/\text{cm}^2$  interacted with the membrane. Loading a grating area of  $1.8 \times 10^{-6} \text{ cm}^2$  with more than  $10^7 \text{ e}^-$  leads to a surface charge density of about  $5 \times 10^{12} \text{ e}^-/\text{cm}^2$ . Thus, an effect on the interference pattern was expected, but did not occur in the experimental data. However, it is not clear whether the gratings would have kept their charge after a year of treatment under air conditions and whether interference would anyhow be possible with such a high charge density at the gratings surface. The theoretical treatment by our colleagues at the University in Rostock concluded that the existing discrepancy between the evaluation of the interference data and the theoretical prediction could be explained with an average charge of one electron per grating bar seen by the molecular wave during its propagation through the grating. Thus, it is necessary to perform further measurements on this topic or using conducting membranes when using gratings milled by focused ion beam technique for interferometry experiments.

### 4.3 Pressure dependent diffraction

A molecule traveling through a vacuum chamber held at a low pressure has a certain probability to hit  $N_2$ ,  $O_2$  or other rest gas particles. Such a collision will lead to scattering of the molecule, which washes out the interferogram. From this effect it is possible to deduce the effective scattering cross section of the molecule.

To analyze interference as a function of pressure we followed the approach in [19, 52]. We start from the law of *A. Beer* and *J. H. Lambert* [71], which describes the transmission  $T$  of a beam through a material by the ratio of its final and initial intensity  $I$  and  $I_0$ , respectively. It can be rewritten in terms of the effective absorption cross section  $\sigma$ , the number of absorbing particles  $N$  per unit volume and the length of the absorbing material  $l$ .

$$T = \frac{I}{I_0} = e^{-\sigma l N} \quad (4.3)$$

From that one derives the fringe visibility of an interferogram depending on the gas pressure in the vacuum chamber as

$$V(p) = V_0 \cdot \exp\left(-\frac{2l\sigma^{\text{eff}}}{k_B T} p\right), \quad (4.4)$$

where  $V_0$  is 1 for data normalized to the intensity at the lowest pressure. It depends on the effective scattering cross section of the molecule  $\sigma^{\text{eff}}$  and the pressure of the colliding gas  $p$  at a fixed temperature  $T$ .

The experimental technique includes some inaccuracies, such as the calibration of the pressure sensors or the actual size of an air particle. Each of those lead to an error in the scattering cross section of the phthalocyanine particle. Thus we compare the result to those of a different data analysis method. To do so, we use scattering theory to get a reasonable estimate for the mean free path

$$\lambda_{\text{mfp}}(p) = \frac{k_B T}{\sqrt{5}\pi(r_1 + r_2)^2 p}, \quad (4.5)$$

with  $k_B$  being the Boltzmann constant,  $p$  the pressure at temperature  $T$  and  $r$  the effective scattering radii of the corresponding particles. The factor of  $\sqrt{5}$  counts the

fact that the air particles are in average twice as fast as the phthalocyanine molecules. When the mean free path of the molecule is large enough to allow it to travel through the whole vacuum chamber, a signal rises at the detector. For lower pressure and longer mean free paths the signal at the detector should increase.

## Measurements and Results

A series of data were taken for phthalocyanine molecules at pressures between  $2 \times 10^{-6}$  mbar and  $4 \times 10^{-8}$  mbar. The visibility of the first order diffraction peaks relative to the first order minimum of the interferogram was taken and evaluated with formula (4.4).

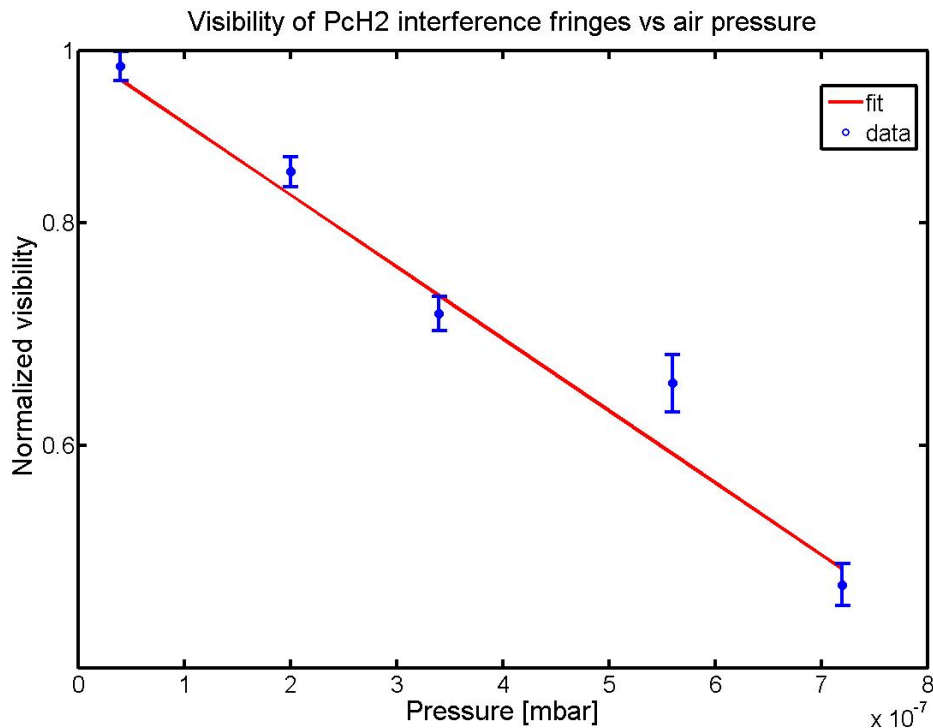


**Figure 4.12** Visibility of the first order interference fringes as a function of the air pressure in the vacuum chamber. The data was normalized to the interference pattern at  $4 \times 10^{-8}$  mbar.

Fitting the data to the theory (as shown in 4.12) results in an effective scattering cross section for phthalocyanine of

$$\sigma_{\text{eff}} \approx 200 \pm 40 \text{ nm}^2,$$

which means, that in a collision of phthalocyanine with an air particle a radius of  $r = 8.0 \pm 3.6$  nm has to be taken into account. Note that the geometrical radius of the molecule is in the order of one nanometer, but does not play a role in this physical interaction. For a comparison to the method of the mean free path we take the total intensity of the zeroth order diffraction signal and extrapolate it to the point, where the signal gets zero. The molecules in the zeroth order diffraction peak will be those that must have had a mean free path clearly above the length of the setup. The knowledge of the pressure which corresponds to this mean free path enables to calculate the radius of the opponents in the scattering process. Assuming  $N_2$  molecules with a *van der Waals* radius of 260 pm we are able to estimate the scattering cross section of phthalocyanine for the signal reduction with a radius of about  $1.9 \pm 0.6$  nm. For the evaluation of the pressure where no signal contributes to the zeroth order a drop below the background signal is essential (see figure 4.13).

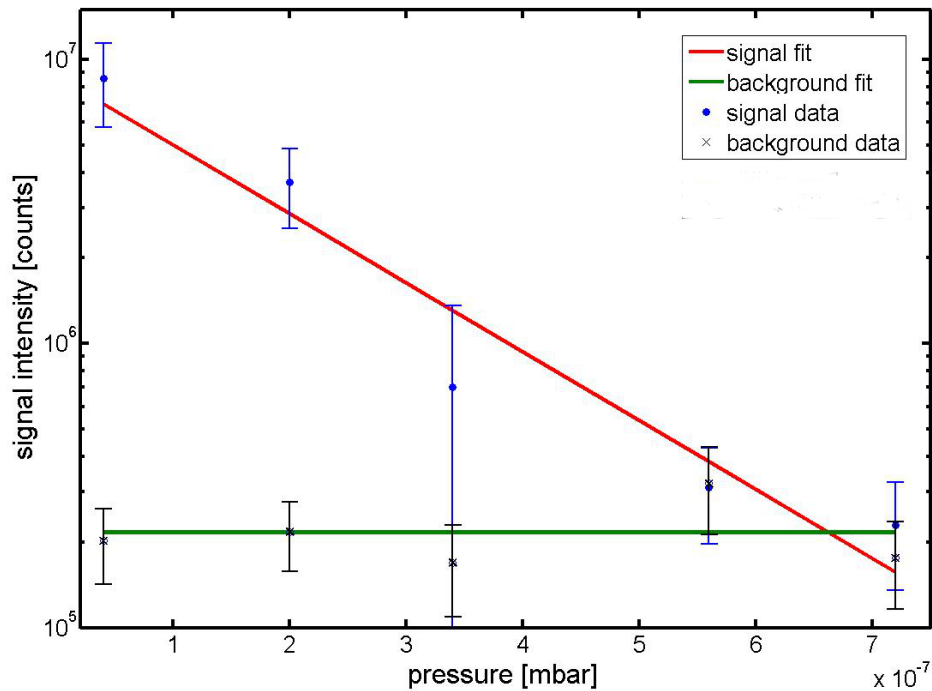


**Figure 4.13** Dependence of the signal intensity of the zeroth order diffraction peak on the pressure in the vacuum chamber. The point where the signal drops below the background intensity defines the critical pressure for 2.1 m mean free path (as defined in 4.5) of the molecule. The statistical error from the fit of the interference peak intensity was below 5 percent for all data points.

Thus, the interaction radius of the particle with air might be a bit bigger due to a nonzero background signal and is expected to lie in between both results.

# 5 Outlook

## 5.1 Atomically thin diffraction gratings: graphene

The effect of *van der Waals* forces in a setup with material gratings should depend on the time the molecule needs to pass the diffracting structure (see formula (2.23)). For a given beam velocity this time changes if the grating thickness is varied. A good understanding of such forces makes it necessary to probe different grating thicknesses. Thin gratings are a technical issue and of particular interest, because they should limit the *van der Waals* interaction to the smallest possible value. The thinnest conceivable grating is a structure written into a single layer of atoms. Graphene appears as the ideal solution. Note, that the electronical structure of graphene is very special. In two dimensions the free electrons travel ballistically. Such effects may have to be taken into account for a theoretical evaluation.

Measurements are currently performed using double and single layer graphene gratings. The first generation of such gratings can be seen in 5.1. Due to the fact, that they are built from a single atomic layer the effective opening fraction does not shrink so much when the grating is rotated. This means that the interaction between molecules and grating bars is the smallest geometrical possible. This will open possibility of rotating a mechanical grating up to 80 degrees or more. Compared to normal incidence a 5 to 6 times wider splitting of the interference maxima is possible. A population of much higher diffraction orders is expected when the effective slit width is reduced. Regarding formula (2.2) and (2.15) the increase in resolution of the interference may be used to increase the mass of the diffracted particle.

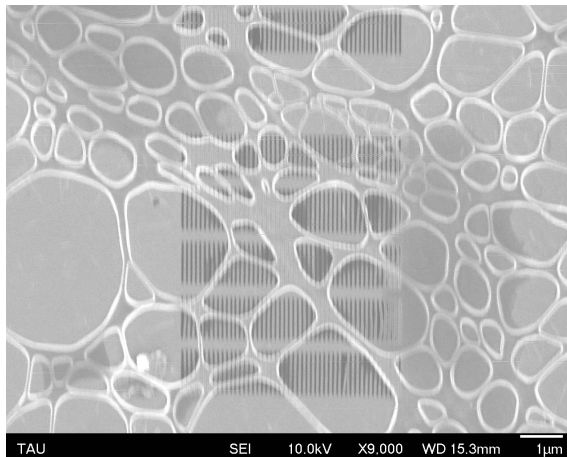


**Figure 5.1** Scanning electron micrograph of a nanograting milled into a double layer of graphene. The graphene layer is suspended over a lacy carbon support structure.

This effect can be combined with a smaller grating periodicity, which would allow for projected geometrical grating periods smaller than 20 nm. Using molecules travelling at a speed of 200 m/s an enhancement of usable masses would go up to 10.000 u with this technique.

## 5.2 Light gratings for a new type of diffraction

In atomic as well as in molecular interference experiments structures made of light have been used [72,73] also to avoid *van der Waals* interactions.

A completely new approach would be the realization of photo-isomerization gratings. A light grating may be used to switch between conformational states of the molecule (figure 5.2). Transitions between these states occur in the UV range. One could make use of different physical properties of these states [74,75] for detecting alternatively the molecules that have not switched in the anti-nodes of the light grating or those that have switched. This can be achieved via a difference in the fluorescent quantum yield between the *trans* and the *cis* state, or a dipole moment that only occurs in one of the states. Two molecules that may be good candidates for such a grating are retinal and resveratrol. The latter is referred to increase its quantum yield after irradiation in the UV range [75].

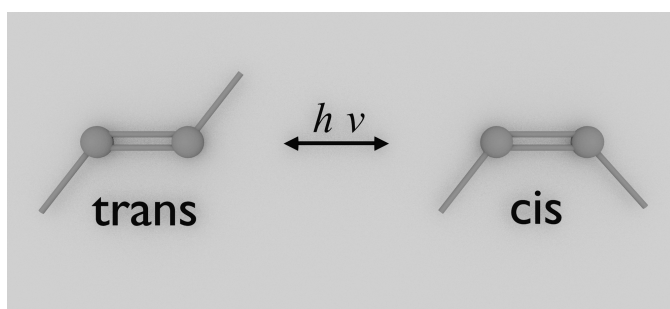


**Figure 5.2** Schematic representation of photo switching between the *trans* and the *cis* state of the molecule.

## 6 Conclusion

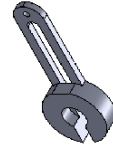
Since *Louis de Broglie* the concept of matter wave duality, one of the fundamental aspects of quantum science has evolved very fast. Nowadays the objects that are investigated get bigger and bigger and experiments in the nano-scale are feasible. Being able to do experiments presupposes the knowledge about the nano-scale systems one is working with. In this context the interaction between a grating and different types of molecules was investigated using molecular diffraction. The grating was rotated with respect to the direction of the molecular beam. For non polar molecules this resulted in a population of higher order interference peaks. In contrast to that the behavior of polar particles indicates the presence of an unusually strong interaction and requires further study.

The scattering cross section of phthalocyanine molecules was studied with this setup using two different approaches for the data evaluation delimiting the radius of the molecule between 1.9 nm and 8.0 nm. Several open questions in this area have to be answered in future experiments, such as gratings built by a single atomic layer or gratings acting in the regime of molecular isomerization.

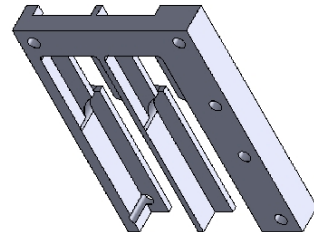
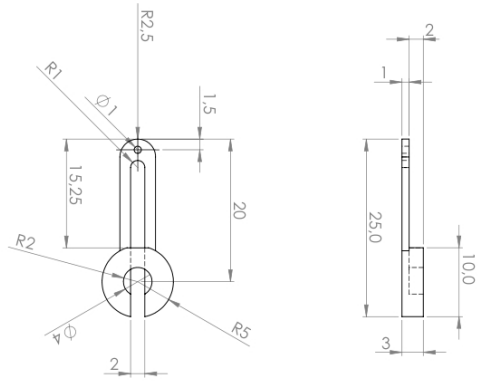
Let me finish this work with a quote of the poet Alexander Pope: “*Nature and Nature’s laws lay hid in night: God said, Let Newton be! and all was light.*” Fortunately he was not right and nature’s laws still lie at least partly in the night. For me this is the reason to work on the general understanding of our world. Nowadays experiments might be a bit more specific than watching an apple fall and the conclusions of it are not of that fundamental importance for our daily life, but still the results are significant bricks in a physical framework. I hope, that with this work I was able to contribute to the one or the other brick as well.

# 7 Appendix

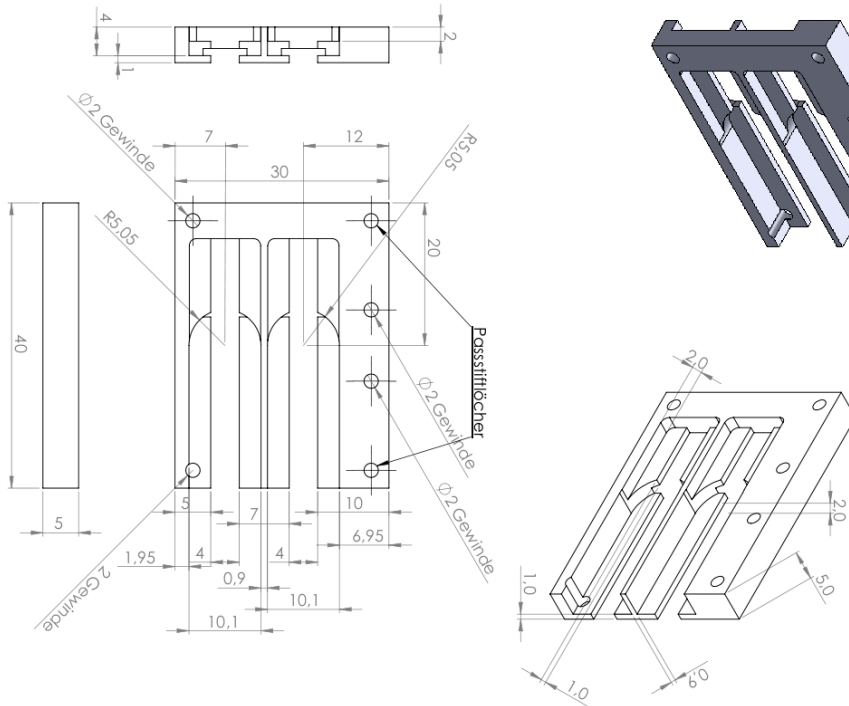
## 7.1 Technical drawings



GRATING BASE



BASE PICKUP



christian.knobloch@uniwlv.ac.at  
06888226849  
ARNDT GROUP

christian.knobloch@uniwlv.ac.at  
06888226849  
ARNDT GROUP

Figure 7.1

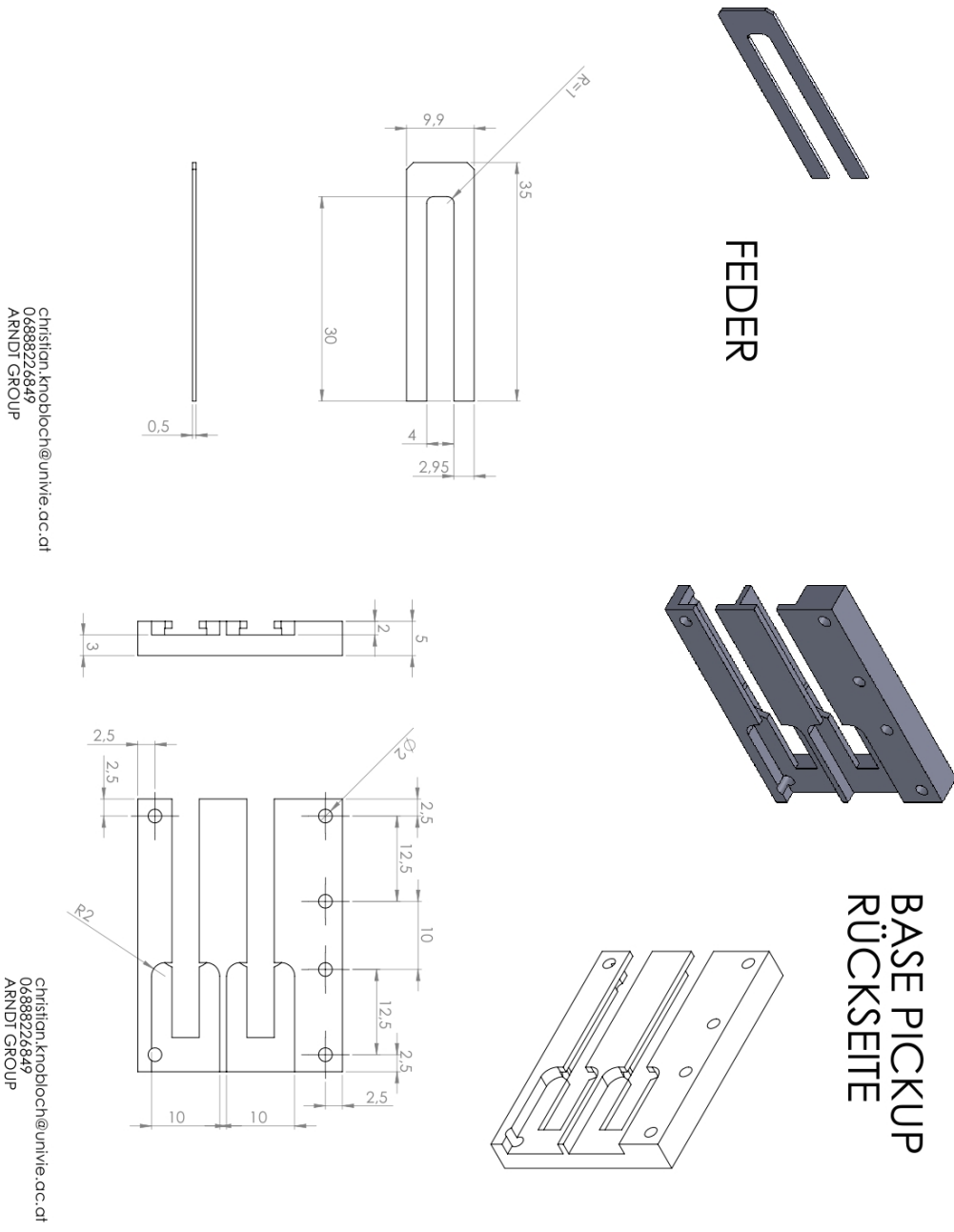


Figure 7.2

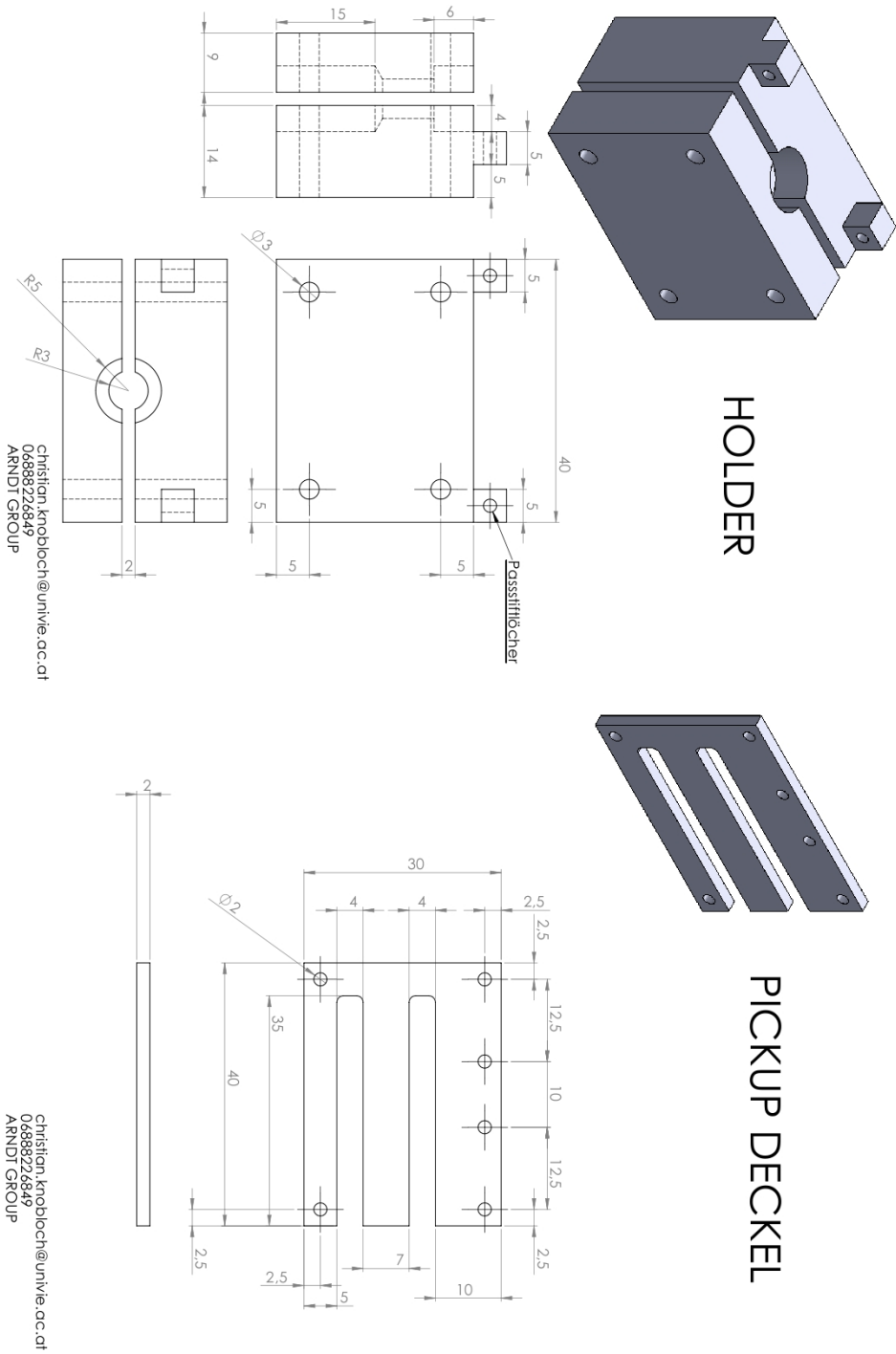


Figure 7.3

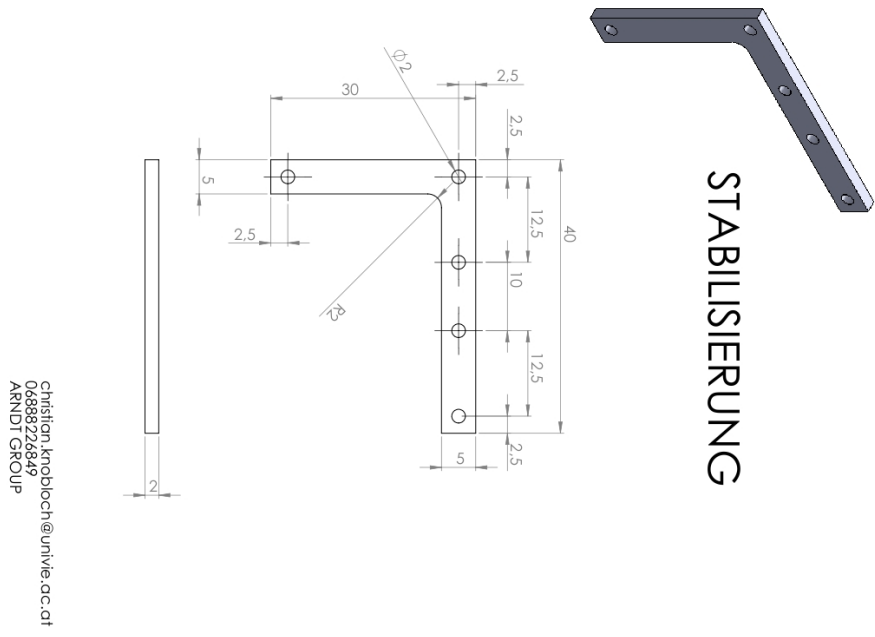


Figure 7.4

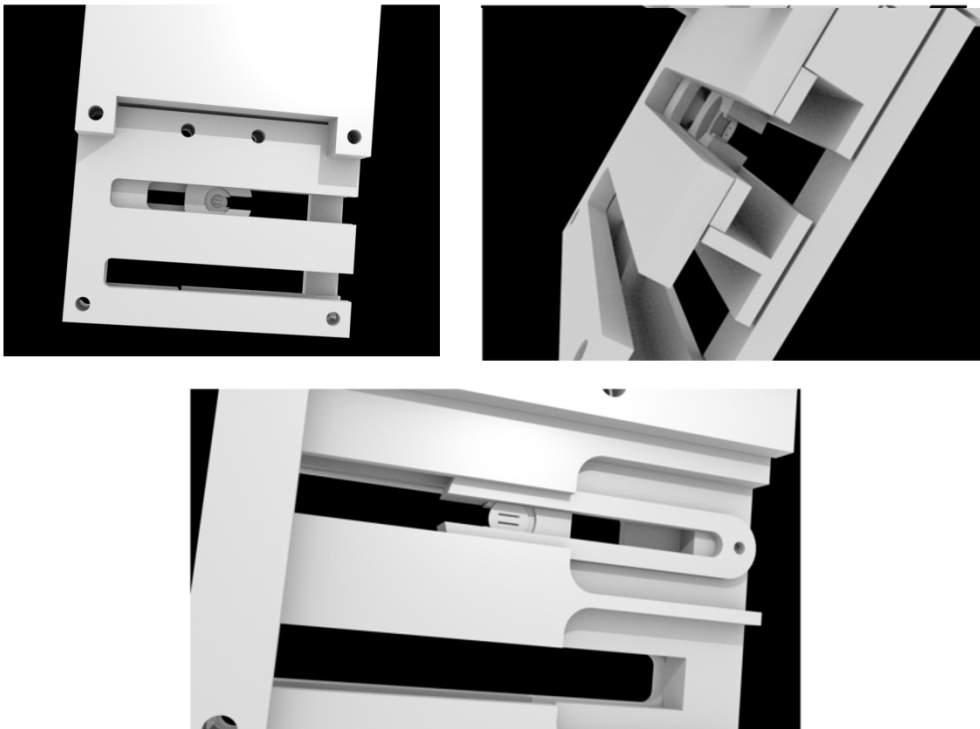


Figure 7.5

## 8 Bibliography

- [1] L. de Broglie; *Waves and Quanta*; Nature 112, No. 2815, 540 (1923)
- [2] C. Davisson and L.H. Germer; *The scattering of electrons by a single crystal of Nickel*; Nature 119, No.2998, 558-560 (1927)
- [3] H. Rauch and S.A. Werner; *Neutron Interferometry-Lessons in experimental quantum mechanics*; Oxford Science Publications (2000)
- [4] H. Rauch; *Neutroneninterferometrie: Schlüssel zur Quantenmechanik*; Physik in unserer Zeit 29, No.2, 56-60 (1998)
- [5] S. A. Werner; *Gravitational, Rotational and Topological Quantum Phase Shifts in Neutron Interferometry*; Class. Quantum Grav. 11, No. 6A, A207-A226 (1994)
- [6] S. Sponar, J. Klepp, K. Durstberger-Rennhofer, R. Loidl, S. Filipp, M. Lettner, R.A. Bertlmann, G. Badurek, H. Rauch, Y. Hasegawa; *Geometric Phase in entangled Systems: A single-neutron Interferometer Experiment*; Phys. Rev. A 81, 042113 (2010)
- [7] P.R.Berman; *Atom Interferometry*; Academic Press (1997)
- [8] B.S. Zhao, S.A. Schulz, S. A. Meek, G. Meijer, W. Schöllkopf; *Quantum reflection of helium atom beams from a microstructured grating*; Phys. Rev. A 78, 010902 (2008)
- [9] J. Fujita, F. Shimizu; *Atom manipulation using atomic de Broglie waves*; Materials Science and Engineering:B 96, No. 2, 159-163 (2002)
- [10] T.Juffmann, H.Ulbricht, M.Arndt; *Experimental methods of molecular matter-wave optics*; Rep. Prog. Phys. 76, No.8, 086402:1:28 (2013)
- [11] L. Hackermüller, S. Uttenthaler, K. Hornberger, E. Reiger, B. Brezger, A. Zeilinger, M. Arndt; *Wave Nature of Biomolecules and Fluorofullerenes*; Phys. Rev. Lett. 91, Nr. 9, 090408 (2003)

- [12] T. Juffmann, A. Milic, M. Müllneritsch, P. Asenbaum, A. Tsukernik, J. Tüxen, M. Mayor, O. Chesnovsky, M. Arndt; *Real-time single-molecule imaging of quantum interference*; Nature Nanotechnology 7, 297-300 (2012)
- [13] S. Gerlich, L. Hackermüller, K. Hornberger, A. Stibor, H. Ulbricht, M. Gring, F. Goldfarb, T. Savas, M. Müri, M. Mayor, M. Arndt; *A Kapitza-Dirac-Talbot-Lau interferometer for highly polarizable molecules* Nature Physics 3, 711-715 (2007)
- [14] S. Nimmrichter, K. Hornberger; *Macroscopicity of Mechanical Quantum Superposition States*; Phys. Rev. Lett. 110, 160403 (2013)
- [15] S. L. Adler, A. Bassi; *Is Quantum Theory Exact?* ; Science 325, 275-276 (2009)
- [16] S. Nimmrichter, K. Hornberger, P. Haslinger, M. Arndt; *Testing spontaneous localization theories with matter-wave interferometry*; Phys. Ref. A 83, 043621 (2011)
- [17] S. Eibenberger, S. Gerlich, M. Arndt, M. Mayor and J. Tüxen; *Matter-wave interference with particles selected from a molecular library with masses exceeding 10,000 amu*; Phys. Chem. Chem. Phys. 15, 14696-14700 (2013)
- [18] S. Gerlich, M. Gring, H. Ulbricht, K. Hornberger, J. Tüxen, M. Mayor, M. Arndt; *Matter-Wave Metrology as a Complementary Tool for Mass Spectrometry*; Angew. Chem. Int. Ed. 47, No. 33, 6159-6198 (2008)
- [19] L. Hackermüller, K. Hornberger, B. Brezger, A. Zeilinger, M. Arndt; *Decoherence in a Talbot-Lau interferometer: the influence of molecular scattering*; Appl. Phys. B 77, No. 8, 781-787 (2003)
- [20] Max Planck; *Ueber das Gesetz der Energieverteilung im Normalspectrum*; Annalen der Physik 309, No. 3, 553-563, (1901)
- [21] W. Wien; *Temperatur und Entropie der Strahlung*; Annalen der Physik 288, No. 5, 132-165 (1894)
- [22] A. Einstein; *Über einen die Erzeugung und Verwandlung des Lichtes betreffenden heuristischen Gesichtspunkt*; Annalen der Physik 322, No. 6, 132-148 (1905)

- [23] W. Heisenberg; *Über den anschaulichen Inhalt der quantentheoretischen Kinematik und Mechanik*; Zeitschrift für Physik 43, Nr. 3-4, 172-198 (1927)
- [24] P. Szriftgiser, D. Guery-Odelin, M. Arndt, J. Dalibard; *Atomic Wave Diffraction and Interference Using Temporal Slits*; Phys. Rev. Lett. 77, Nr. 1, 4-7 (1996)
- [25] O. Nairz, M. Arndt, A. Zeilinger; *Experimental verification of the Heisenberg uncertainty principle for fullerene molecules*; Phys. Rev. A 65, 032109 (2002)
- [26] E. Schrödinger; *An undulatory theory of the mechanics of atoms and molecules*; Phys. Rev. 28, No. 6, 1049-1070 (1926)
- [27] N. Wiener; *Generalized harmonic analysis*; Acta Mathematica 55, No. 1, 117-258 (1930)
- [28] A. Chintchin; *Korrelationstheorie der stationären stochastischen Prozesse*; Mathematische Annalen 109, No. 1, 604-615 (1934)
- [29] P.H. van Cittert; *Die Wahrscheinliche Schwingungsverteilung in Einer Lichtquelle Direkt Oder Mittels Einer Linse Beleuchteten Ebene*; Physica 1, No. 1-6, 201-210 (1934)
- [30] F. Zernike; *The concept of degree of coherence and its application to optical problems*; Physica 5, No. 8 785-795 (1938)
- [31] E. Hecht; *Optik*; Oldenburg Verlag, 4. Auflage (2002)
- [32] W. H. Zurek; *Decoherence and the Transition from Quantum to Classical—Revisited*; Progress in Mathematical Physics 48, 1-31 (2002)
- [33] D. M. Bacon; *Decoherence, Control, and Symmetry in Quantum Computers*; Ph.D. thesis, University of California, Berkeley (2001)
- [34] M. Born, E. Wolf; *Principles of optics*; Pergamon Press (1993)
- [35] V. P. A. Lonij, W. F. Holmgren, A. D. Cronin; *Magic ratio of window width to grating period for van der Waals potential measurements using material gratings*; Phys. Rev. A 80, 062904 (2009)

- [36] T. Juffmann, S. Nimmrichter, M. Arndt, H. Gleiter, K. Hornberger; *New Prospects for de Broglie Interferometry*; Found. Phys. 42, No. 1, 98-110 (2012)
- [37] F. Hasselbach; *Progress in electron- and ion-interferometry*; Rep. Prog. Phys. 73, No. 1, 016101 (2010)
- [38] I. Pikovski, M. Zych, F. Costa, C. Brukner; *Universal decoherence due to gravitational time dilation*; arXiv:1311.1095v1 [quant-ph]
- [39] R. Brühl, P. Fouquet, R. E. Grisenti, J. P. Toennies, G. C. Hegerfeldt, T. Köhler, M. Stoll, C. Walter; *The van der Waals potential between metastable atoms and solid surfaces: Novel diffraction experiments vs. theory*; Europhys. Lett. 59, No. 3, 357-363 (2002)
- [40] J. D. Perreault, A. D. Cronin; *Measurement of atomic diffraction phases induced by material gratings*; Phys. Rev. A 73, 033610 (2006)
- [41] S. Lepouture, V.P.A. Lonij, H. Jelassi, G. Trenec, M. Büchner, A. D. Cronin, J. Vigue; *Atom interferometry measurement of the atom-surface van der Waals interaction*; Eur. Phys. J. D 62, 309-325 (2011)
- [42] R. E. Grisenti, W. Schöllkopf, J. P. Toennies; *Determination of Atom-Surface van der Waals Potentials from Transmission-Grating Diffraction Intensities*; Phys. Rev. Lett. 83, Nr. 9, 1755-1758 (1999)
- [43] F. London; *The general theory of molecular forces*; Transactions of the Faraday Society 33, 8-26 (1937)
- [44] J. Israelachvili; *Intermolecular and Surface Forces*; Academic Press Limited (1991)
- [45] S. Y. Buhmann, S. Scheel, S. A. Ellingsen, K. Hornberger, A. Jacob; *Casimir-Polder interaction of fullerene molecules with surfaces*; Phys. Rev. A 85, 042513 (2012)
- [46] I. E. Dzyaloshinskii, E. M. Lifshitz, L. P. Pitaevskii; *General theory of van der Waals forces*; Soviet Physics Uspekhi 73, 153-76 (1961)
- [47] H. B. G. Casimir, D. Polder; *The influence of Retardation on the London-van der Waals Forces*; Nature 158, 787-788 (1946)

- [48] V. Mostepanenko, N. N. Trunov; *The Casimir Effect and its Applications*; Oxford Science Publications (1997)
- [49] A. D. Cronin, J. D. Perreault; *Phasor analysis of atom diffraction from a rotated material grating*; Phys. Rev. A 70, 043607 (2004)
- [50] Z. Gan, Y. Cao, R.A. Evans and M. Gu; *Three-dimensional deep sub-diffraction optical beam lithography with 9nm feature size*; Nature Communications 4, 2061 (2013)
- [51] Michele Sclafani ; *Molecular beam methods for quantum optics experiments: sources, detection schemes and coherent manipulation*; Dissertation, Fakultät für Physik, Universität Wien (2013)
- [52] K. Hornberger, S.Uttenthaler, B. Brezger, L. Hackermüller, M. Arndt, A. Zeilinger; *Collisional Decoherence Observed in Matter Wave Interferometry*; Phys. Ref. Lett. 90, 160401 (2003)
- [53] T.Juffmann; *Surface based detection schemes for molecular matter wave interferometry*; Dissertation, Fakultät für Physik, Universität Wien (2013)
- [54] S.Yogev, J. Levin, M. Molotsky, A. Schwarzmann, O. Avayu, Y. Rosenwaks; *Charging of dielectrics under focused ion beam irradiation*; Journal of Applied Physics 103, 064107 (2008)
- [55] P. Sonnentag; *Ein Experiment zur kontrollierten Dekohärenz in einem Elektronen-Biprisma-Interferometer*; Dissertation, Fakultät für Mathematik und Physik, Eberhard-Karls-Universität, Tübingen (2006)
- [56] S. Scheel, S. Y. Buhmann; *Path decoherence of charged and neutral particles near surfaces*; Phys. Rev. A 85, 030101 (2012)
- [57] P. Haslinger, N. Dörre, P. Geyer, J. Rodewald, S. Nimmrichter, M. Arndt; *A universal matter-wave interferometer with optical ionization gratings in the time domain*; Nature Physics 9,144–148 (2013)
- [58] E. Abbe; *Beiträge zur Theorie des Mikroskops und der mikroskopischen Wahrnehmung.*; Archiv für mikroskopische Anatomie 9, No. 1, 413-418 (1873)

- [59] R. E. Thompson, D. R. Larson, W. W. Webb; *Precise Nanometer Localization Analysis for Individual Fluorescent Probes*; Biophys. Journal 82, 2775-2783 (2002)
- [60] S. R. P. Pavani, M. A. Thompson, J. S. Biteen, S. J. Lord, N. Liu, R. J. Twieg, R. Pietsun, W. E. moerner; *Three-dimensional, single-molecule fluorescence imaging beyond the diffraction limit by using a double-helix point spread function*; PNAS 106, No. 9, 2995-2999 (2009)
- [61] T. Schmidt, G. J. Schütz, W. Baumgartner, H. J. Gruber, H. Schindler; *Imaging of single molecule diffusion*; Proc. Natl. Acad. Sci. USA 93, 2926-2929 (1996)
- [62] A. Schob, F. Cichos; *A Modified Surface Forces Apparatus for Single Molecule Tracking*; J. Phys. Chem. B 110, 4354-4358 (2006)
- [63] S. Ramadurai, A. Holt, V. Krasnikov, G. v. d. Bogaart, J. A. Killian, B. Poolman; *Lateral Diffusion of Membrane Proteins*; J. Am. Chem. Soc. 131, 12650-12656 (2009)
- [64] Y. Y. Kievsky, B. Carey, S. Naik, N. Mangan, D. ben-Avraham, I. Sokolov; *Dynamics of molecular diffusion of rhodamine 6G in silica nanochannels* The Journal of Chemical Physics 128, 151102 (2008)
- [65] A. T. Gradyushko, A. N. Sevchenko, K. N. Solovyov and M. P. Tsvirko; *Energetics of photophysical processes in chlorophyll-like molecules*; Photochem. Photobiol. 11, 387-400 (1970)
- [66] R. F. Kubin and A. N. Fletcher; *Fluorescent quantum yields of some rhodamine dyes*; J. Luminescence 27, 455-462 (1982)
- [67] S. K. Tripathi, A. Monga and G. S. Saini; *Characterization of thermally evaporated thin films of Rhodamine 6G*; Smart Mater. Struct.18, No. 12, 125012 (2009)
- [68] J. C. Delgado, R. G. Selsby; *Density Functional Theory Calculations on Rhodamine B and Pinacyanol Chloride. Optimized Ground State, Dipole Moment, Vertical Ionization Potential, Adiabatic Electron Affinity and Lowest Excited Triplet State*; Photochemistry and Photobiology 89, 51-60 (2013)
- [69] NIST Mass Spectrometry Data Center; *Rhodamine B*; National Institute of Standards and Technology, NIST MS number 236163 (2011)

- [70] G. Scoles, D. Bassi, U. Buck, D. Laine; *Atomic and molecular beam methods, Volume 1*; Oxford University Press (1988)
- [71] A. Beer; *Bestimmung der Absorbtion des roten Lichts in farbigen Flüssigkeiten*; *Annalen der Physik* 162, No. 5, 78–88, 1852 (1852)
- [72] O. Nairz, B. Brezger, M. Arndt, A. Zeilinger; *Diffraction of complex molecules by structures made of light*; *Phys. Rev. Lett.* 87, 160401 (2001)
- [73] P. J. Martin, B. G. Oldaker, A. H. Miklich, and D. E. Pritchard; *Bragg scattering of atoms from a standing light wave*; *Phys. Rev. Lett.* 60, 515–518 (1988)
- [74] I. Yang et al.; *Photochemical generation of a new, highly fluorescent compound from non-fluorescent resveratrol*; *Chemical Communications* 48, No. 32, 3839-3841 (2012)
- [75] A. Feis et al.; *Role of the Triplet State in Retinal Photoisomerization as studied by Laser-Induced Optoacoustic Spectroscopy*; *Journal of Physical Chemistry B* 101, No.38, 7620-7627 (1997)

## Illustrations

In the following a list of the figures, that were not originally made by the author, and their license holder is given.

- [i] Figure 3.12: Scott Prah: Oregon Medical Laser Center (08.06.2014)
- [ii] Figure 3.13: Scott Prah: Oregon Medical Laser Center (08.06.2014)
- [iii] Figure 3.15: Scott Prah: Oregon Medical Laser Center (08.06.2014)
- [iv] Figure 3.16: Scott Prah: Oregon Medical Laser Center (08.06.2014)
- [v] Figure 3.18: Scott Prah: Oregon Medical Laser Center (08.06.2014)
- [vi] Figure 3.19: Scott Prah: Oregon Medical Laser Center (08.06.2014)
- [vii] Figure 4.8: Dr. Christian Brand
- [viii] Figure 5.1: Dr. Michele Sclafani, taken at the University of Tel Aviv

## 9 Acknowledgements

*"Not everything that can be counted counts, and not everything that counts can be counted." - Albert Einstein.*

In the following lines I want to thank for having people around me who know about the difference and all those people without whom this work would not have been possible.

First of all I want to thank Univ.-Prof.Dr.Markus Arndt, who gave me the wonderful opportunity to finish my master in such an inspiring scientific surrounding. I want to thank him also for many fruitful discussions and for spending much of his precious time in supporting me. In that context I also want to mention Dr. Michele Sclafani, who taught me a lot about scientific work and often pushed me in the enhancement of my skills. Especially him , Dr. Christian Brand, Dr. Thomas Juffmann and also all the other kind members of our research group I want to thank for a nice time and a lot of interesting discussions. In this way let me also express my respect to the whole quantum physics group in Vienna for the way young students get included into scientific work.

Let me also thank my sister, who inspired me to study physics at the University of Vienna and my whole family for their backing. Especially let me thank my parents who enabled me studying and not only financially supported me during the time of my education. Deepest thanks for that.

## Curriculum vitae



### Christian Gerald Knobloch, BSc

date of birth: 03.05.1989 in Melk  
place of residence: Aggsbach-Dorf 119, 3642 Aggsbach-Dorf  
citizenship: Austria  
phone nr.: 0688/8226849  
e-mail: christian.knobloch@univie.ac.at

### Education

from 1995 to 1999: *Elementary school* in Aggsbach-Dorf  
from 1999 to 2003: *Stiftsgymnasium* in Melk  
from 2003 to 2007: *High school at the Abbey of Melk*  
focused on visual art  
from 2007 to 2008: Civil service (*Zivildienst*) at the *Red Cross* in Melk  
from 2008 to 2012: Bachelor Study of Physics at the University of Vienna  
since 2012: Master Study of Physics at the University of Vienna

### Personal skills and competences

since January 2008: Paramedic competence and volunteer practice for the *Red Cross*.  
during summer 2010: Creation of a solution book for the math-book of the sixth grade for the *Veritas Verlag*.  
since October 2013: Employment as project staff in the group of Prof. Markus Arndt.

### Publications

- M. Sclafani, T. J. Juffmann, C. Knobloch, M., Arndt; *Quantum coherent propagation of complex molecules through the frustule of the alga Amphipleura pellucida*; New Journal of Physics 15, 083004 (2013)

